

Computational model and sensitivity study of
transepithelial/transendothelial electrical resistance for
optimizing *in vitro* models of cell barriers

Alda Profka

Department of Bioengineering & Biomedical Engineering
McGill University, Montréal

April 12, 2023

A thesis submitted to McGill University in partial fulfillment of the requirements of the degree of

Biological & Biomedical Engineering program

©2023 Alda Profka

Abstract

Transepithelial/transendothelial electrical resistance (TEER) is a parameter widely used for monitoring the barrier integrity of an endothelial cell layer in *in vitro* models. Measuring TEER is a non-invasive and label-free technique that allows for fast and continuous measurements. Although it would be expected to obtain comparable TEER values for the same cell type and conditions, the reported values across the literature vary considerably. To account for differences stemming from specific measurement-related effects, finite element models (FEM) of conventional transwell culture inserts and an in-house microfluidic chip design were created using COMSOL. The microfluidic chip contains four electrodes integrated on each side of the porous membrane without hindering the field of view. It accounts for small changes in temperature or medium composition by deriving the isolated TEER independent of channel properties. The model was experimentally validated by measuring the TEER of a polyester membrane at different electrode positions. The results show the importance of using a geometric correction factor to find the true value of TEER based on the contribution of each zone of the cell layer to

cautiously interpret the resulting data. The percentage difference between the simulated and theoretical TEER value represents the error in the measurement. Moreover, the FEM models were used to identify the most and least sensitive geometric and electrical parameters to electrical resistance. By considering the sensitivity distribution and the ranking of the model parameters derived from the numerical simulations, efficient and trustworthy methods can be developed to assess and study the cellular barrier functions. Future microfluidic models containing barrier-forming tissue are expected to be of great value for disease modeling, drug development, and precision medicine. Physiologically-relevant humanoid models can help advance our understanding of pathological conditions such as cancer, several psychiatric and neurodegenerative diseases, and other inflammatory diseases, as well as significantly lower the time and cost of bringing new drugs to the market.

Abrégé

La résistance électrique transépithéliale/transendothéliale (TEER) est un paramètre largement utilisé pour surveiller l'intégrité de la barrière d'une couche de cellules endothéliales dans des modèles *in vitro*. La mesure du TEER est une technique non invasive et sans étiquette qui permet des mesures rapides et continues. Bien qu'on s'attende à obtenir des valeurs TEER comparables pour le même type de cellule et les mêmes conditions, les valeurs rapportées dans la littérature varient considérablement. Pour tenir compte des différences résultant d'effets spécifiques liés à la mesure, des modèles d'éléments finis (FEM) des inserts de culture transwell conventionnels et une conception de puce microfluidique interne ont été créés à l'aide de COMSOL. La puce microfluidique contient quatre électrodes intégrées de chaque côté de la membrane poreuse sans gêner le champ de vision. Il tient compte des petits changements de température ou de composition du milieu en dérivant le TEER isolé indépendamment des propriétés du canal. Le modèle a été validé expérimentalement en mesurant le TEER d'une membrane en polyester à différentes positions d'électrodes. Nos résultats montrent l'importance d'utiliser un facteur

de correction géométrique pour trouver la vraie valeur de TEER en fonction de la contribution de chaque zone de la couche cellulaire pour interpréter avec prudence les données résultantes. La différence en pourcentage entre la valeur TEER simulée et théorique représente l'erreur de mesure. De plus, les modèles FEM ont été utilisés pour identifier les paramètres géométriques et électriques les plus et les moins sensibles à la résistance électrique. En considérant la distribution de sensibilité et le classement des paramètres du modèle dérivés des simulations numériques, des méthodes efficaces et fiables peuvent être développées pour évaluer et étudier les fonctions de barrière cellulaire. Les futurs modèles microfluidiques contenant des tissus formant une barrière devraient être d'une grande valeur pour la modélisation des maladies, le développement de médicaments et la médecine de précision. S'ils sont appliqués avec succès, les modèles humanoïdes peuvent aider à faire progresser notre compréhension des conditions pathologiques telles que le cancer, plusieurs maladies psychiatriques et neurodégénératives et d'autres maladies inflammatoires, ainsi qu'à réduire considérablement le temps et le coût de mise sur le marché de nouveaux médicaments.

Acknowledgements

The completion of this Master's would not have been possible without the guidance and support of my supervisor, Dr. Luc Mongeau, my research team, and my family and friends. Please accept my sincere gratitude for the endless encouragement and wise counsel.

I am also grateful to the Department of Biological & Biomedical Engineering at McGill University for providing me with the resources to pursue graduate studies. I had the pleasure of collaborating with many talented faculty members and fellow graduate students. Lastly, special thanks to the COMSOL technical support team who spent their time instructing me and the Natural Sciences and Engineering Research Council of Canada (NSERC) for their support.

Contents

Abstract	i
Abrégé	iii
Acknowledgements	v
1 Introduction	1
1.1 Background	1
1.1.1 <i>In vivo</i> , <i>in vitro</i> and <i>in silico</i> models	4
1.1.2 Transepithelial/transendothelial electrical resistance measurements	6
1.1.3 Organs-on-a-chip devices for TEER measurement	13
1.2 Impact	15
1.3 General literature review	16
1.3.1 Blood-brain barrier models	17
1.4 Resistance models	23
1.5 History	28
1.6 Research aims	30

2	COMSOL simulations of sensitivity distribution in <i>in vitro</i> models	33
2.1	Introduction	33
2.1.1	Literature review	35
2.1.2	Theoretical background	37
2.2	Methodology	38
2.2.1	Model definition	38
2.2.2	Modeling considerations	41
2.2.3	Mesh refinement	42
2.2.4	Simulation of electrical potential	44
2.2.5	Sensitivity field distribution	45
2.2.6	Geometric correction factor evaluation	46
2.3	Results and discussion	47
2.3.1	Mesh Refinement	47
2.3.2	Sensitivity distribution	48
2.3.3	Geometric correction factor	53
2.3.4	Influence of electrode placement on TEER values in transwells	56
3	Experimental validation and parameter ranking	57
3.1	Background	57
3.2	Methodology	59
3.2.1	Mold 3D printing	59

3.2.2	Fabrication of the organ-on-chip device	59
3.2.3	Modeling Considerations	61
3.2.4	Data analysis	63
3.3	Results and Discussion	65
3.3.1	Parameter ranking	65
4	Discussion and Conclusions	69
4.1	Limitations	72
4.2	Future directions	73
4.3	Broader implications	74

List of Figures

- 1.1 Simplified BBB schematic showing how targeted UIMD enhances cellular uptake of hydrophobic drugs by affecting the cell membrane. Adapted from Cho et al. [2002] 3
- 1.2 Barrier formed by an endothelial cell layer with an equivalent circuit model. R_a and R_b represent the apical and basolateral cell membrane resistance, respectively. R_{tj} is the resistance of the tight junctions, R_{ic} the intercellular resistance, and R_{gap} the gap resistance. Adapted from Odijk et al. [2015] 8
- 1.3 A) The EVOM/Millicell ERS-2 unit with an STX2/ “chopstick” electrode pair placed in a traditional transwell culture system. B) The equivalent circuit includes the resistance of the cell layer, $TEER$, the electrode medium interface, R_{EMI} , the porous membrane, R_{PM} , and the cell culture medium, R_{medium} , in series. 10

1.4	A) Schematic of the microfluidic device with two electrodes on each side of the membrane. B) Cross-sectional schematic of the membrane with the cellular monolayer. C) Equivalent circuit diagram where R_{1-4} represent the resistance of the medium and the electrode medium interface, and R_{M+EC} the resistance of the membrane and the cell monolayer. The electrodes are represented by E1, E2, E3, and E4. Adapted by van der Helm et al. [2016]	27
2.1	Schematics of the 3D model simulation design for A) 24-well plate transwell with insert diameter of 6.5 mm B) 12-well plate transwell with insert diameter of 12 mm C) 6-well plate transwell with insert diameter of 24 mm D) microfluidic chip designed by [van der Helm et al., 2016] E) in-house microfluidic chip	39
2.2	A) Cross-sectional geometrical model and mesh of the 24-well plate transwell system (insert of 6.5 mm in diameter). The simulated model mostly depends on the volume between the electrodes where the electrical current density is confined, whereas the rest of the system has a negligible effect on the measurement. B) Comparison of the mesh pre- and post-adapted mesh refinement. C) Element quality histogram for element skewedness pre- and post-adapted mesh refinement.	43

-
- 2.3 Current density norm [A/m^2] along the cell culture area shown in 2D sections when TEER is obtained in a transwell culture insert using STX2 electrodes (model A), in a microfluidic model of van der Helm et al. (model B), and our in-house microchip model (model C). Results are presented for different insert diameters (6.5 mm and 12 mm) and different channel heights (0.300, 0.475, and 0.650 mm) for TEER equal to a) $1 \Omega cm^2$ b) $10 \Omega cm^2$ c) $100 \Omega cm^2$ d) $1000 \Omega cm^2$ 49
- 2.4 Sensitivity profile of the cell barrier along the dashed line axis shown in Fig. 2.3 in a transwell culture insert using STX2 electrodes (model A). Results are presented for different insert diameters (6.5 mm in red and 12 mm in yellow) and TEER values: A) $1 \Omega cm^2$ B) $10 \Omega cm^2$ C) $100 \Omega cm^2$ D) $1000 \Omega cm^2$ 50
- 2.5 Sensitivity profile of the cell barrier along the dashed line axis shown in Fig. 2.3 in a microfluidic model as designed by van der Helm et al. (model B). Results are presented for different channel heights (0.300mm in yellow, 0.475 mm in red, and 0.650 mm in blue) and TEER values: A) $1 \Omega cm^2$ B) $10 \Omega cm^2$ C) $100 \Omega cm^2$ D) $1000 \Omega cm^2$ 51
- 2.6 Sensitivity profile of the cell barrier along the dashed line axis shown in Fig. 2.3 in our in-house microchip model (model C). Results are presented for different channel heights (0.300mm in yellow, 0.475 mm in red, and 0.650 mm in blue) and TEER values: A) $1 \Omega cm^2$ B) $10 \Omega cm^2$ C) $100 \Omega cm^2$ D) $1000 \Omega cm^2$. 52

2.7 A) B) C) Error [%] and D) E) F) GCF when TEER is obtained in a transwell insert of diameter 6.5 and 12 mm (model A) and in the microfluidic models (model B & C) for different microchannel heights (0.300mm in yellow, 0.475mm in red, and 0.650 mm in blue). 54

List of Tables

1.1	TEER values for BBB models.	24
2.1	Geometrical input parameters for electrical simulations.	40
3.1	Electrical input parameters for electrical simulations.	62
3.2	Geometrical input parameters for electrical simulations.	62
3.3	Cotter's simulation cases for a five-parameter model. High and low parameter values are indicated by H and L, respectively.	64
3.4	Importance value statistics obtained from Cotter's method. R_t refers to the total resistance, R_m to the membrane resistance, and $A \cdot R_m$ to the membrane resistance normalized to the area. The parameters consist of the conductivity of the media, σ_{r-m} , the conductivity of the cell barrier, σ_{r-cb} , the microchannel height, h_r , the microchannel width, w_r , and the penetration depth, d_r	66

-
- 3.5 Statistics for local sensitivity values. R_t refers to the total resistance, R_m to the membrane resistance, and $A \cdot R_m$ to the membrane resistance normalized to the area. The parameters consist of the conductivity of the media, σ_{r-m} , the conductivity of the cell barrier, σ_{r-cb} , the microchannel height, h_r , the microchannel width, w_r , and the penetration depth, d_r 67

List of Acronyms

16HBE14o-	human bronchial epithelial cells.
AC	alternating current.
AIC	air interface condition.
ATI	alveolar epithelial type I cells.
BBB	blood-brain barrier.
CAD	computer-aided design.
CNS	central nervous system.
DC	direct current.
EVOM	epithelial volttohmmeter.
FEM	finite element method/models.
GCF	geometric correction factor.
GP8	cerebral cortex endothelial cell.
HBMECs	primary human brain microvascular endothelial cells.
hCMEC/D3	immortalized human cerebral endothelial cell.

hiPSCs	human induced pluripotent stem cells.
IS	impedance spectroscopy.
LCC	liquid-covered condition.
NPCs	neuronal progenitor cells.
RBE4	rat brain microvessel endothelial cell.
TEER	transepithelial/transendothelial electrical resistance.
TJ	tight junction.
UIMD	ultrasound-induced mild hyperthermia.

Chapter 1

Introduction

1.1 Background

One characteristic feature of epithelial and endothelial cells in multicellular organisms is the formation of selectively permeable interfaces that separate compartments of different chemical compositions and control substance exchange. Adjacent cells of these epithelial/endothelial cell layers are connected by different protein complexes, with the so-called tight junctions (TJs) being the most prominent representative. TJs are intercellular connections that secure barrier integrity by regulating ion and molecular diffusion across the barrier, as well as guiding intracellular transport processes [Benson et al., 2013]. The apical and basolateral sides of the barrier are formed by the polarization of the cells, which is enabled by transmembrane protein complexes and different lipid compositions.

The barrier integrity is pivotal in maintaining the physiological activities of the surrounding tissue microenvironment. Its impairment has been found to play a significant role in several psychiatric and neurodegenerative diseases, cancer, pulmonary and intestinal inflammatory diseases, age-related macular degeneration, and many other pathological conditions. Modulation of the barrier can promote barrier opening, preserve barrier integrity, or restore barrier closure, and has become an active area of research with the potential to help us understand its contribution to pathogenesis and how to fight it [Claesson-Welsh et al., 2021]. The barrier is not static when subjected to specific stimuli, such as exposure to certain substances, laser or direct current stimulation, and ultrasound propagation among others [Li et al., 2021, Pouliopoulos et al., 2020, Shin et al., 2020]. The blood-brain barrier (BBB), located in the central nervous system (CNS), is the tightest and most selective endothelial barrier and serves to protect the brain from the unwanted actions of substances circulating in the blood [Langen et al., 2019]. In many neurological disorders, such as brain trauma and tumors, cerebral ischemia, and neurological diseases, the BBB permeability is augmented [Wilhelm et al., 2011]. Examples of deliberate manipulations of the BBB for therapeutic applications include a temporary increase in permeability by ultrasound-induced mild hyperthermia (UIMD) to allow polar drugs to reach the brain as shown in Figure 1.1 [Cho et al., 2002], or a decrease in permeability by regular physical exercise to reduce inflammation [Abbott, 2000].

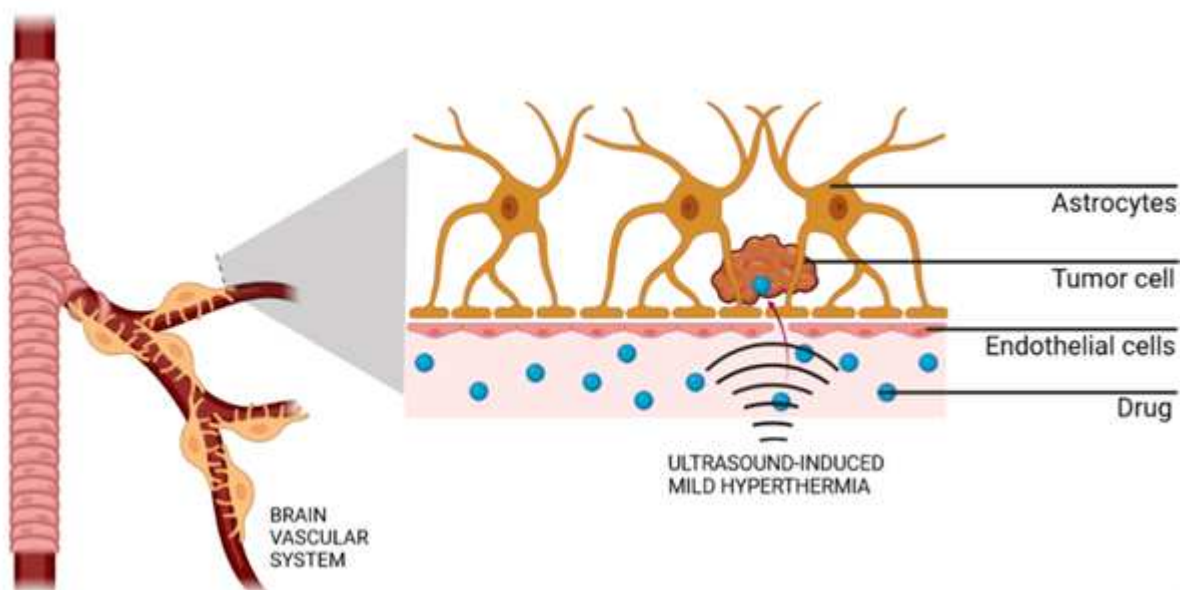


Figure 1.1: Simplified BBB schematic showing how targeted UIMD enhances cellular uptake of hydrophobic drugs by affecting the cell membrane. Adapted from Cho et al. [2002]

1.1.1 *In vivo, in vitro* and *in silico* models

Various *in vivo*, *in vitro*, and *in silico* models are employable to investigate barrier function, integrity and development during maturation and assess drug permeability. However, there are limitations associated with each one. Being able to study the organ of interest in its natural environment is the main advantage of *in vivo* experiments. Several injection techniques are used to calculate the permeability-surface area product [mL/(min·g)], which is a reliable measurement of the unidirectional clearance across the barrier – from blood to brain in the case of BBB [Pardridge, 2004]. Imaging techniques, including magnetic resonance imaging, positron emission tomography, and single-photon emission computed tomography, may be used alongside to evaluate transport properties, as well as diagnose various diseases [Nicolazzo et al., 2006]. Laboratory animals are used to perform these studies, but it has been shown that approximately 50% of results collected from these models are not translatable to human responses [Perel et al., 2007]. Additionally, a lot of people look down upon the use of animals in scientific research mainly because of obvious ethical reasons, such as animal abuse. According to a study conducted by Pew Research Center in 2015, almost 1 in 4 college graduates with a science degree in the US oppose the practice [NW et al., 2015].

To overcome ethical and scientific concerns, *in vitro* and *in silico* models are employed. Although results acquired on cell monolayers correlate poorly with *in vivo* BBB

permeability values, *in vitro* methods are advantageous because of a relatively greater throughput, early identification in case of toxicity, lower cost, full access to both the apical and the basolateral compartments, as well as the ability to measure the compound directly in buffer and assess the corresponding transport mechanisms [Lundquist et al., 2002]. Generally, a porous polyester or polycarbonate membrane is seeded with epithelial or endothelial cells in between two microfluidic channels, which represent the luminal and abluminal compartments. These models are based on primary cell or cell lines' cultures grown on permeable supports and are used to study cell barrier function or measure its permeability. To mimic the *in vivo* situation, models used for drug permeation studies require adequately restrictive TJs that hinder paracellular transport. Measuring the permeability of certain markers through immunostaining is a commonly used method to determine the integrity of these *in vitro* models. However, the use of macromolecular fluorescent tracers is time-consuming, labor-intensive, and can interfere with the analysis. Transepithelial/ transendothelial electrical resistance (TEER) measurements are a more straightforward and non-invasive method to confirm the presence of an intact barrier and monitor barrier formation and function *in vitro* in real-time. Different methods of measuring TEER are further discussed in this paper.

Finally, *in silico* models or finite element models (FEM) can be applied to better monitor specific characteristics of barrier-forming monolayers and to allow for comparison of TEER values across different organ-on chip platforms. Numerical simulations of FEM models enable

the user to restrain a large dataset of compounds into a smaller set of lead compounds, thus reducing the large number of variables stemming from the physiological or/and pathological complexity.

1.1.2 Transepithelial/transendothelial electrical resistance measurements

The electrical resistance of the cell layer has been the most frequently used parameter to assess the integrity of endothelium and was first introduced by Crone et al. to measure BBB properties of various species *in vivo* [Crone and Christensen, 1981]. Measuring TEER across a cell layer and a cell culture membrane is a relatively low-cost and non-invasive method that provides real-time quantitative information on the status and tightness of a cellular barrier *in vitro* without the need of slow-diffusing fluorescent markers. Most current flows between cells at low frequencies due to the capacitance of the cell membranes. Therefore, TEER usually represents the impedance to the transport of ions and molecules across the epithelium, thus being an indicator of paracellular ion passage. However, at higher frequencies, both the paracellular and transcellular path contribute to the overall impedance. The simplified electrical circuit model for TEER measurement [Odijk et al., 2015] represents the electrical resistance of the paracellular and transcellular pathways in parallel (Fig. 1.2). The transcellular pathway resistance, R_{trc} , is equal to the sum of the apical and the basolateral cell membrane resistance, R_a and R_b ,

whereas the resistance of the paracellular pathway, R_{pc} , is depicted by the sum of the tight junction resistance, R_{tj} , and the intercellular resistance, R_{ic} . The equivalent resistance, Ξ , is given by

$$\Xi = R_{trc} // R_{pc} = \frac{(R_a + R_b) \cdot (R_{tj} + R_{ic})}{(R_a + R_b) + (R_{tj} + R_{ic})}. \quad (\text{Eq. 1})$$

A decrease in TEER indicates an impairment of barrier function and an increase in permeability. Partial cell coverage over the supporting substrate is represented by the gap resistance, R_{gap} , and is an important factor (Fig. 1.2). A gap as small as 0.4% of the cell support can significantly reduce the measured TEER by 80% [Odiijk et al., 2015]. TEER measurements have a wide range of applications, such as determining the culture day with the optimum tightness for experiments, establishing the baseline permeability on individual filters, or following the effects of a particular pharmacological agent, drug, or growth factor on TJ function and barrier integrity over time [Abbott et al., 2014]. It is used in both traditional transwell culture systems and in organs-on-chips. The measurements can be conducted across the cell layer at a single frequency (0-100 Hz) or using electrical impedance spectroscopy (IS) (10 Hz-1 MHz).

TEER Measurements based on Ohm's Law

To measure TEER, a direct current (DC) or an alternating current (AC) square-wave current is applied through the electrodes, one on each side of the cell layer to

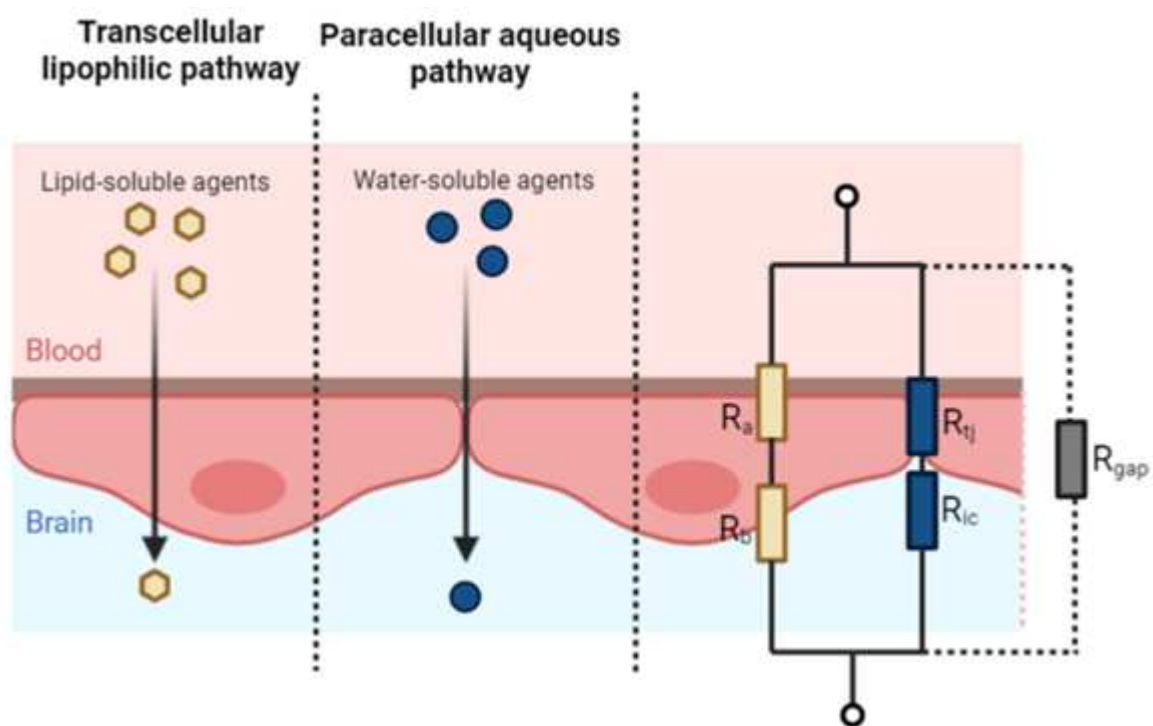


Figure 1.2: Barrier formed by an endothelial cell layer with an equivalent circuit model. R_a and R_b represent the apical and basolateral cell membrane resistance, respectively. R_{tj} is the resistance of the tight junctions, R_{ic} the intercellular resistance, and R_{gap} the gap resistance. Adapted from Odijk et al. [2015]

measure the resulting current upon the applied potential. An AC voltage source is preferable over DC, as it avoids polarizing effects on the electrodes and charging of the cell layer. The Electrical Voltohmmeter (EVOM) system or the equivalent Millicell® ERS-2 (Electrical Resistance System) are widely cited and recommended instruments and are considered to be the standard method for TEER acquisition. These instruments provide membrane potential and TEER measurement values of cell monolayers by using a pair of electrodes named the STX2 or “chopstick” electrode pair (Fig. 1.3). Millicell® ERS-2 works by passing a constant current of 10 μA through the membrane and reversing the polarity 12.5 times per second between the two current-injecting electrodes. After measuring the voltage required to reach the applied current through the companion electrodes, the ohmic resistance, R , is calculated according to Ohm’s law. The resistance of a sample without cells, R_{blank} , as well as the resistance of a sample seeded with the cell monolayer, R_{total} are measured during this procedure. The cell-specific resistance, R_{cells} , is calculated as the difference of R_{total} and R_{blank} as

$$R_{cells} = R_{total} - R_{blank}. \quad (\text{Eq. 2})$$

The effective surface area of the membrane, A , reported in units of cm^2 , is inversely proportional to the resistance since an increased area would provide more effective paths for current to pass. To compare TEER measurements among different experimental setups,

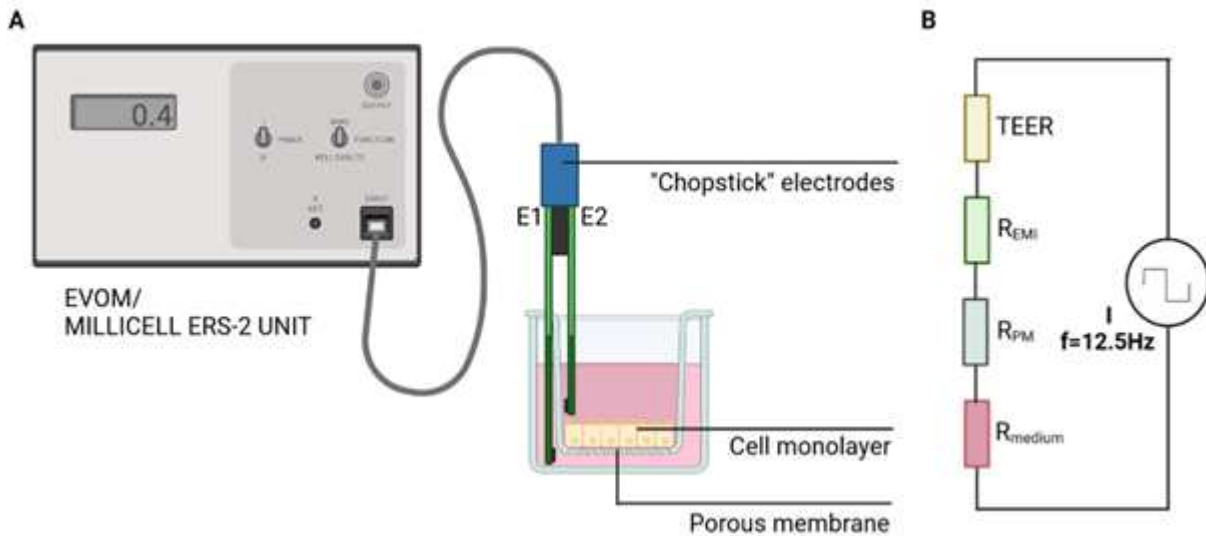


Figure 1.3: A) The EVOM/Millicell ERS-2 unit with an STX2/ “chopstick” electrode pair placed in a traditional transwell culture system. B) The equivalent circuit includes the resistance of the cell layer, $TEER$, the electrode medium interface, R_{EMI} , the porous membrane, R_{PM} , and the cell culture medium, R_{medium} , in series.

the electrical resistance, reported in units of Ωcm^2 , is normalized to the area by multiplying R_{cells} by the effective membrane area using

$$TEER(\Omega\text{cm}^2) = R_{cells}(\Omega) \cdot A(\text{cm}^2). \quad (\text{Eq. 3})$$

This formula indicates that the whole area contributes equally to the measurement. Although this convention has been widely adopted for decades, it has lately been shown to be subject to error since the geometry, the electrode placement, and the caused vibrations during measurements can lead to inhomogeneity of the electric field across the epithelium [Jovov et al., 1991]. The STX2 electrodes have a chopstick-like arrangement,

each one consisting of a silver/silver chloride (Ag/AgCl) pellet at the tip and a silver wire positioned at the edge. The use of STX2 electrodes has been associated with a non-uniform distribution of current density across the cellular monolayer especially in 6-well plates leading to a systematic overestimation of TEER [Jovov et al., 1991]. Thus, the latter model was excluded from our studies. Errors in the resulting TEER values can be caused by a change of position of the probing electrodes during measurements since the device is handheld and must be manually positioned for measurements. The unequal distribution of the current flow is thought to be one of the main reasons for non-ohmic electrical responses and inconsistent resistance values across *in vitro* platforms.

The top and bottom electrodes of EndOhm chambers from World Precision Instruments (WPI) Inc. are fixed at a central position inside, minimizing the variability caused by electrode positioning and gap, thus giving more accurate and reproducible results. The STX2 electrode system generally gives 20-40% higher readings in large transwell inserts of 24 mm diameter from 6-well plates, when compared to the EndOhm chamber [Wang et al., 2017]. However, the results obtained from the latter are nearly the same to those from smaller transwell inserts of 6.5 mm or 12 mm diameter, indicating a uniform electrical field in those cases [Wang et al., 2017]. Another disadvantage of measuring TEER in transwell inserts is the disruption of the physiological conditions when the cell cultures are temporarily removed from the incubator as it can result on a change of cell medium temperature and concentration. All things considered, this technical approach holds a significant risk of providing erroneous

results, and it is highly recommended to independently verify the measurements obtained by it.

Impedance Spectroscopy

A cell barrier has capacitive and resistive effects. As abovementioned, the cells connected by TJs can form a barrier and control the ionic and molecular flux across the intercellular space. The gaps at the cell-cell junctions govern the paracellular resistance or TEER. The impermeability of charged substances through the cells' phospholipid membrane causes the capacitive effects. The capacitance of a cell membrane is measured to be around $1 \mu\text{F}/\text{cm}^2$ but morphological characteristics of the cell membranes that affect the membrane surface area, as well as the composition and the thickness of the cell layer can change the capacitance value [Linz et al., 2020]. For example, microvilli formation can increase the membrane surface area and hence increase the capacitance of the cell layer, whereas higher organization or expression of TJs can lead to better cell alignment accompanied by smooth cell borders which would reduce the membrane surface area and the capacitance [Czupalla et al., 2014]. Therefore, tight barriers have low capacitance values and high TEER values.

Impedance spectroscopy is another method used for TEER measurements that overcomes many limitations of DC resistance methods. IS combined with a suitable algorithm can better represent the values compared to traditional DC or single-frequency

AC measurement methods [Douville et al., 2010]. It works by changing the input signal from direct to alternating currents with varying frequency and it can provide us with cell capacitance values arising from the electrically insulating lipid bilayer membranes. The main purpose of this measuring system is to signal when the cells are completely confluent in a continuous monolayer and can be harvested and used for further experiments. The cellZscope® device (nanoAnalytics) is a computer-controlled measurement system, which allows the monitoring during growth and differentiation of barrier-forming cell cultures in standard transwell inserts, providing cell capacitance values as well as TEER ones. Alternatively, a potentiostat or galvanostat along with fitting algorithms can be used to define the resistive and capacitive properties.

1.1.3 Organs-on-a-chip devices for TEER measurement

The current commercial systems used for measuring TEER are generally limited to macroscopic and static cellular environments. Cells cultured in transwell inserts encounter a phenotypical shift, because of the two-dimensional (2D) nature of the assay, as well as the absence of physiological conditions, such as the lack of proper interactions with other cells and the extracellular matrix (ECM) and shear stress acting on the cell barrier through fluid flow. Moreover, the presence of the supports in the transwell cultured cells hinders observation by light microscopy. Organs-on-chips systems are *in vitro* models, microengineered to represent improved biomimicry relative to other *in vitro* culture

methods. These models can precisely control the mechanical and biochemical factors in the cellular microenvironment and introduce physiologically relevant fluid flow conditions and shear stress. Introducing these stresses to certain cell types has shown to induce mechanotransductive effects i.e., regulating transport processes in a kidney model [Duan et al., 2008].

Organs-in-chips generally contain microfluidic channels and chambers occupied by living cells. The aim is to reproduce key functional and structural components of living human tissues or organs to recapitulate the complex physiological conditions *in vitro*. The electrodes used are custom designed, usually made of platinum (Pt) or Ag/AgCl pellets, and their size is scaled relative to the microchannel dimensions. They are inserted or embedded into the chip system to achieve measurements in much smaller surface areas relative to traditional culture systems. It is important to make sure that there is a uniform current density across the cell monolayer during TEER measurement. Electrical simulations can be used to ensure equal distribution of the current flow from the chosen electrode design process.

Recently, there is a growing interest in developing organs-on-chips due to the above-mentioned scientific and ethical reasons. These *in vitro* cell barrier models can be used to perform permeability and drug transport studies in the early stages of drug discovery. They have the potential to provide a cost-effective, reliable, and high-throughput method for modeling disease and studying transport phenomena and drug interactions in a humanoid model while reducing reagent consumption. Microfluidic systems can also

provide control over applied physiologic stresses, degree of cell-cell interaction, and chemical signaling [Atencia and Beebe, 2005, Walker et al., 2004]. Developing a single *in vitro* system that represents all the *in vivo* conditions may not be possible, but a variety of *in vitro* systems that closely mimic the characteristics of the barrier integrity of the *in vivo* tissue can be used for decision-making in early drug discovery. Effective screening of drug candidates can be remarkably facilitated by establishing high-fidelity *in vitro* models.

1.2 Impact

The integrity of a cell barrier is important for many biological processes as well as in drug delivery. The development of medicines that can reach the brain is one of the greatest challenges in the pharmaceutical industry. Epithelial barriers found in other systems such as the intestine, the kidney, the lungs, the skin, and the placenta are also a subject of interest when it comes to developing targeted drug delivery strategies. According to recent analyses, it takes approximately \$1.3 billion and 9.1 years to bring an experimental compound from the lab bench to the market [Brown et al., 2021, DiMasi et al., 2016]. In the current drug development process, *in vivo* screening is carried out in the preclinical phase, which is found to be time-consuming and highly expensive. The reliance on testing drugs in laboratory animals before they are tested on humans is a major cause of the high costs and time spent on drug development. Because of the mismatch in biology, many toxic or ineffective drugs advance through clinical trials at large costs, while potentially

effective drugs don't make it to market. Consequently, there is an extensive interest shown by many pharmaceutical, cosmetic, and food industries to apply efficient high-fidelity *in vitro* models or organs-on-chips for evaluating the absorption and potential toxic effects of different drugs, xenobiotics, and nutrients, respectively. Furthermore, World Health Organization (WHO) Global status report states that the annual worldwide cost of dementia alone was above US\$ 1.3 trillion in 2019, which represented 1.5% of the global GDP at that time [status report, 2021]. Considering the aging population, these numbers are anticipated to increase to US\$ 2.8 trillion by 2030 [status report, 2021]. Since BBB dysfunction is associated with Alzheimer's disease, multiple sclerosis, stroke, brain tumors, epilepsy among others, regulating its function is regarded as a promising therapeutic target for treating these diseases [Weiss et al., 2009].

1.3 General literature review

TEER has been incorporated in many studies concerning epithelial tissues, including drug delivery, the integrity and metabolism of intestinal mucosa, the permeability of the BBB, the response of TJ to proinflammatory cytokines, identifying other factors affecting the development of TJs, and investigating ion transport pathways across an epithelial layer among others [Srinivasan et al., 2015]. The literature review focuses on BBB models, as they are more widely studied than other models and allow for comparisons to be made among

different techniques and methods. Other barrier models developed to predict drug transport include pulmonary, gastrointestinal, placental, ocular, nasal, skin-based, and vaginal.

1.3.1 Blood-brain barrier models

The barrier between the blood and the brain is composed of an elaborate network of vascular endothelial cells that isolate CNS from systemic blood circulation. It is surrounded by basal lamina, pericytes, microglia, and astrocytic endfeet with astrocytes arranging the cellular link to neurons [Prabhakarbandian et al., 2013]. BBB endothelium is quite distinct because of a combination of physical and biochemical barriers, making it the tightest one in the body. It is characterized by tight junctions, minimal pinocytotic vesicles, and a lack of fenestrations. Anticonvulsants, alcohol, and narcotics, which are small lipid-soluble substances less than 400-500 Da, can pass easily through the BBB. For most other substances, the tight junctions develop a diffusion barrier, preventing the brain from taking any large molecule therapeutics bigger than 1kDa consisting of recombinant protein and genes, as well as 98% of neurotherapeutics consisting of small molecules proteins and peptides of size 500 to 1kDa [Prabhakarbandian et al., 2013]. Numerous potential therapeutics are macromolecular in nature, based on genes, peptides, and recombinant proteins. Thus, it is difficult for them to reach the CNS in relevant concentrations. The development of techniques to make these novel therapeutics cross the BBB is a major challenge that can have a remarkable impact on how we treat several CNS disorders.

The values found in literature for the resistance across the BBB *in vivo* range from 1500 to 8000 Ωcm^2 , as shown on Table 1.1. As reported by Butt et al., the mean TEER across the blood vessel walls on the pial surface of the brain in rats of age 28-33 day old was about 1500 Ωcm^2 [Butt et al., 1990], which is close to values of 1870 Ωcm^2 obtained in corresponding studies on brain surface vessels in frogs [Crone and Olesen, 1982]. The technique developed by Crone and Olesen based on the infinite leaky cable theory [Hodgkin, 1951, Katz, 1966] is the method used for these experiments. Another study calculated a TEER of 8000 Ωcm^2 for brain parenchymal vessels using the combined permeability of radioisotopic potassium, chloride, and sodium in the adult rat [Smith and Rapoport, 2006]. The difference between pial and parenchymal vessels or in the measuring technique may be the cause of this significantly higher value. However, some values close to 5900 Ωcm^2 were also obtained in the same experiments by Butt et al., and it is reasonable to consider these higher figures as the true TEER of the BBB, since any potential deterioration during the preparation can lead to lower measured values.

Some of the challenges associated with building *in vitro* models of the BBB are the low availability of human primary brain microvascular endothelial cells, poor barrier formation by immortalized cells, as well as species differences. Brain endothelial cells originating from mice, rats, pigs, bovines or humans are the most-used primary cell cultures, with hCMEC/D3 (human origin), RBE4, and GP8 (rat origin) being the most well-characterized and retaining essential BBB characteristics [Wilhelm et al., 2011]. The

human brain microvascular endothelial cells (HBMECs) have been found to present the best barrier properties for permeability studies in transwells [Eigenmann et al., 2013]. Immortalized animal cell lines are the most widely used because of the relative ease with which they can be cultured, but most of these models cannot reach TEER values above 300-500 Ωcm^2 . Adding hydrocortisone to the culture has been shown to increase these values up to 1800 Ωcm^2 [Franke et al., 1999]. To increase the accuracy of the *in vitro* models, primary animal cells within the first couple of passages have been used more recently, despite it being a time-consuming and sensitive process as these cells lose phenotypic expressions lacking exposure to physiological factors when cultured *ex vivo*. Other than the cerebral endothelial cells, astrocytes, pericytes, glial cells, and neurons also play important regulatory roles in the upkeep/maintenance of the BBB and can be co-cultured to establish more complex *in vitro* models [Deli et al., 2005].

Monocultures of endothelial cells, usually cultured in astrocyte-conditioned medium, have been shown to be a reasonable and informative model for permeability studies, even though they lack the complexity of physiological conditions *in vivo*. Upon the introduction of microfluidic cell culture systems, there has been a resurgence of monocultures as these systems are limited in the number of cell types they can administer. Presenting the cells to shear stresses through the fluid flow has shown to significantly increase the TEER values. However, transwells are the most widely used platform *in vitro* model, usually using 0.01 mm thick polyester or polycarbonate membranes with 400 nm pores at a density of 10^8

pores/mm². The endothelial cells are generally cultured on the luminal side of the membrane, whereas additional cells, such as astrocytes, pericytes, and/or neurons, are grown on the abluminal compartment or on the bottom of the well in cell-specific growth medium. A transwell model consisting of cultured porcine brain capillary endothelial cells was successful in reaching maximal TEER values after 5 days of differentiation in a serum-free hydrocortisone containing medium, with the values ranging between 1200 and 1800 Ωcm^2 , which is close to the *in vivo* barrier values of 1900 Ωcm^2 [Nitz et al., 2003].

To achieve a more robust *in vitro* barrier, mainly characterized by higher TEER values, endothelial cells are co-cultured with other cell types. Barrier resistance of only primary HBMECs or immortalized hCMEC/D3 cultured in a 12-well plate transwell system was found to be very similar between the two during days 3-10 of culture, averaging 100 Ωcm^2 , but astrocyte co-culture for both cell types yielded significantly higher TEER values ($\approx 140 \Omega\text{cm}^2$) [Daniels et al., 2013]. The co-culture of endothelial cells with astrocytes has been shown to reestablish many BBB features, making astrocytes the most common cell type used for co-cultures. It has been shown that astrocytes are central to the vasodilation of microvessels [Zonta et al., 2003] and can substantially increase TEER values compared with monocultures, especially in cases when the cells are in contact with one another [Nakagawa et al., 2009]. A 2D microfluidic model using BMECs derived from human induced pluripotent stem cells (hiPSCs) co-cultured with rat primary astrocytes on different sides of a porous membrane achieved meaningful BBB barrier features, as demonstrated by continuous TJ

formation and high TEER values close to *in vivo* ones [Wang et al., 2017]. The TEER values reached a maximum ($4000 \Omega\text{cm}^2$) on day 3 and were maintained above $2000 \Omega\text{cm}^2$ up to 10 days. The medium fluid was circulated at physiologically appropriate perfusion rates using a rocking platform to minimize wall shear stress and reach relevant shear stress values. Other papers haven't been as successful in reaching these high values for an extended period without the help of other cell types or treatment with various chemicals.

Additional cell types have also been co-cultured with endothelial cells and astrocytes to replicate *in vivo* TEER values. The electrical resistance of a co-culture of endothelial (bovine BMEC or RBE4) cells on the luminal side, rat astrocytes on the abluminal side, and neuronal cells on the bottom of a 6-well plate was assessed with an EndOhm-6 chamber attachment and the Millicell-ERS Voltohmmeter. The BMEC-astrocyte-neuron model reached values of approximately $275 \pm 15 \Omega\text{cm}^2$, whereas the RBE4-astrocyte-neuron model achieved even higher values ($\approx 500 \pm 10 \Omega\text{cm}^2$) [Balbuena et al., 2010]. A fully human BBB model was constructed with hiPSC-derived BMESs, primary human astrocytes and pericytes and neuronal progenitor cells (NPCs)-derived neurons treated with retinoic acid. The optimum co-culture scheme in modified medium reached TEER values as high as $5350 \pm 250 \Omega\text{cm}^2$ and maintained these values at above $3000 \Omega\text{cm}^2$ for over 3 days [Lippmann et al., 2014]. The models used in most of these studies employ commercially available TEER equipment such as 6- or 12-well transwell inserts and STX2 electrodes.

Great efforts have been put forward the development and improvement of these BBB models; starting from building simplistic *in vitro* 2D systems to more realistic 2D and 3D microfluidic platforms that can precisely control the mechanical and biochemical factors in the microenvironment. The goal is to mimic the *in vivo* environment in the most accurate way possible. A biomimetic dynamic real-scale BBB model was fabricated through two-photon lithography to create capillary diameter size microtubes [Marino et al., 2018]. These porous microtubes are used as scaffolds for co-culturing U87 glioblastoma cells and bEnd.3 endothelial cells and allow for transport of substances toward the external environment. Even though the TEER values measured were significantly low ($75 \pm 2 \Omega\text{cm}^2$) relative to other systems discussed in this review, the study proposes the first biohybrid 1:1 scale 3D model with microcapillary diameter size and *in vivo*-like fluid flows. Suggested ways to increase the TEER in this system include co-culturing endothelial cells with other cell types, treating the cells with specific molecules (e.g., hydrocortisone), chemicals (e.g., retinoic acid) or serum-free astrocyte conditioned-medium, and applying shear stress.

Because of the small scale of these systems and other design limitations, custom-built electrodes are integrated or placed into the system with minimal disturbance of the cellular environment. However, integrated electrodes can limit visual inspection of the cellular barrier, whereas the insertion of the electrodes into the chip's outlets can lead to erroneous results because of the high resistance of the medium-filled microchannels. Moreover, small changes in temperature or composition of the medium or in the placement of the electrodes

can remarkably affect the TEER measurements. A microfluidic chip using four electrodes inserted into two channels on each side of the membrane can derive the isolated TEER independent of the microchannel properties through six measurement configuration system [van der Helm et al., 2016]. The apparent TEER of a hCMEC/D3 monolayer averaged $22 \pm 1.3 \Omega\text{cm}^2$, which is significantly different from values reported for hCMEC/D3 cells ($\approx 100 \Omega\text{cm}^2$) cultured in a 12-well transwell system and measured by commercially available STX2 electrodes [Daniels et al., 2013]. Therefore, there is a need for checking the validity of these models and cautiously interpreting the resulting data.

A comparison between the BBB model system qualities and review of the current work using immortalized and primary cell cultures is shown on Table 1.1. It should be considered that readings may also differ depending on the method used to measure TEER; STX2 electrodes in transwells, EndOhm cup electrodes, or custom electrodes in microchips, other than on cell type choice and experiment conditions.

1.4 Resistance models

In the traditional setup for measurement of TEER, a cell monolayer is cultured in a semipermeable filter insert, consisting of a porous membrane that is permeable to media and ions. The filter insert separates the apical and basolateral compartments, which are both in contact with a pair of STX2 electrodes. To measure TEER, the shorter leg (E2) of the electrodes is inserted into the media of the upper compartment while being cautious not to

Cell type used	TEER (Ωcm^2)	Equipment used	Reference
BBB (frog, <i>in vivo</i>)	1870	2 microelectrodes (infinite leaky cable theory)	[Crone and Olesen, 1982]
BBB (rat, <i>in vivo</i>)	30 - 5900 (≈ 1500)	2 microelectrodes (infinite leaky cable theory)	[Butt et al., 1990]
BBB (rat, <i>in vivo</i>)	8000	Calculated from the permeability coefficients and the measured plasma concentrations	[Smith and Rapoport, 2006]
Porcine brain capillary endothelial cells	1200-1800	Impedance spectra analyzer/gold film as working electrode in transwell	[Nitz et al., 2003]
Primary HBMECs	100	EVOM/STX2 electrodes in transwell	[Daniels et al., 2013]
hCMEC/D3	100	EVOM/STX2 electrodes in transwell	[Daniels et al., 2013]
hCMEC/D3 + primary human astrocytes	≈ 140	EVOM/STX2 electrodes in transwell	[Daniels et al., 2013]
hBMEC + rat primary astrocytes	4000 (max)	Millicell-ERS/custom + Ag/AgCl electrodes in a 2D microfluidic platform	[Wang et al., 2017]
Bovine BMEC + rat astrocytes + neuronal cells	275 ± 15	Millicell-ERS/EndOhm chamber	[Balbuena et al., 2010]
RBE4 + rat astrocytes + neuronal cells	$\approx 500 \pm 10$	Millicell-ERS/EndOhm chamber	[Balbuena et al., 2010]
hiPSC-derived BMESs + primary human astrocytes and pericytes + NPCs-derived neurons	≈ 5000	EVOM/STX-2 electrodes in transwell	[Lippmann et al., 2014]
bEnd.3 + U87 glioblastoma cells	75 ± 2	Millicell-ERS2/custom electrodes in a 3D real-scale model	[Marino et al., 2018]
hCMEC/D3	22 ± 1.3	Lock-in amplifier with a probe cable circuit operated by LabVIEW/Pt electrodes in a 2D chip	[van der Helm et al., 2016]

Table 1.1: TEER values for BBB models.

touch the cell layer, whereas the longer leg (E1) is placed in the outer well and should meet its bottom (Fig. 1.3A). The total electrical ohmic resistance is usually measured by an EVOM or a Millicell ERS-2 system as described above. An equivalent circuit of this method can be represented by the ohmic resistance of the cell layer, Ξ , the electrode medium interface, R_{EMI} , the resistance of the cell culture medium, R_{medium} , and the resistance of the porous membrane, R_{PM} , in series, where an AC voltage signal with a frequency of 12.5Hz is applied throughout (Fig. 1.3B). The equivalent equation is

$$R_{total} = \Xi + R_{EMI} + R_{medium} + R_{PM}. \quad (\text{Eq. 4})$$

To remove the variability stemming from the electrode medium interface, the medium, and the porous membrane, the resistance measurement of a blank system is subtracted from the measurement of the cellular monolayer-containing system.

Analogous to the conventional transwell system, many developed organs-on-chips use electrodes inserted in the outlets to measure TEER. There is limited reliability associated with this model, because of the small scale of the microchannels and variations arising from electrode reinsertion. We can illustrate this by providing the equation approximating the electrical resistance of an electrolyte in a microfluidic channel,

$$R_{ch} = \rho \frac{l_{ch}}{A_{ch}}. \quad (\text{Eq. 5})$$

Assuming uniform current density, the electric resistance of the medium inside the microfluidic channel, R_{ch} , is proportional to the specific electrical resistance of the medium, ρ , and the length of the channel in meters, l_{ch} , over the cross-sectional area of the channel, A_{ch} . Differences in electrode position during reinsertion can result in a different current density distribution, the presence of non-conductive inhomogeneities such as air bubbles can affect the effective area, and changes in temperature and ion concentration due to evaporation can influence the material properties of the electrolytes. Although changes of non-biological origin are the cause of a different value of the measured TEER, all these variations can add up to incorrectly suggest a change in the cellular barrier tightness.

For our study, we chose to base the design of the microfluidic chip to one with four current-passing electrodes integrated inside the microchannels, two on each side of the membrane [van der Helm et al., 2016]. Using a four-point probe design by separating the voltage measuring and current-passing electrodes, instead of a two-point probe one, helps eliminate the contribution of lead and contact resistances and the electrode-electrode double layer capacitance interference. Furthermore, the four-electrode configuration design allows us to subtract the resistance of paths between electrodes on the same side of the membrane to lower the contribution from the medium and the electrode medium interface to total resistance. There are six combinations to determine the resistance between two electrodes, R_{i-j} , where i and j denote the electrode number. This method can be applied to any organ-on-chip device consisting of two channels separated by a porous membrane. An equivalent

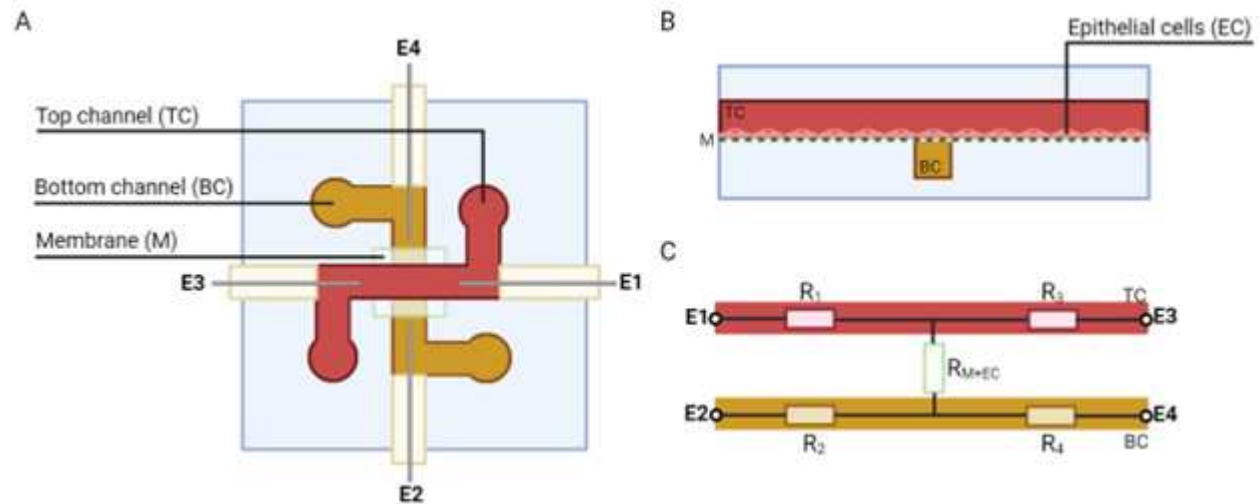


Figure 1.4: A) Schematic of the microfluidic device with two electrodes on each side of the membrane. B) Cross-sectional schematic of the membrane with the cellular monolayer. C) Equivalent circuit diagram where R_{1-4} represent the resistance of the medium and the electrode medium interface, and R_{M+EC} the resistance of the membrane and the cell monolayer. The electrodes are represented by E1, E2, E3, and E4. Adapted by van der Helm et al. [2016]

simplified resistant circuit (Fig. 1.4C) shows how each measured resistance equals the sum of resistances in its path and provides us with a system of six equations and five unknowns, which can be solved by Gaussian elimination.

The TEER is determined by multiplying the effective culture area, A_c and R_{M+EC} , followed by subtracting the TEER of the blank system prior to cell culture $A_c \cdot R_M$. The TEER, Ξ , is equal to

$$\Xi = A_c \cdot R_{M+EC} - A_c \cdot R_M = A_c \cdot \frac{1}{4}(R_{1-2} + R_{1-4} + R_{2-3} + R_{3-4} - 2R_{1-3} - 2R_{2-4}) - A_c \cdot R_M. \quad (\text{Eq. 6})$$

The probe design, the microchannel geometry, and the membrane area must be closely considered as they affect the current distribution across the cellular monolayer, and consequently the TEER measurement accuracy. Other factors affecting TEER include the material, quality, and surface state of the electrodes, the material and porosity of the semipermeable membrane or cell support, its coating, the medium formulation, as well as the cell type(s), confluency, morphology, and conductivity. It is suggested to keep these variables constant during experiments to allow for more accurate values and more precise comparisons.

1.5 History

Electrical methods have been used for over 70 years to characterize tissue permeability in animal models. Since these methods depend on the instantaneous transport of the ionic species across the barrier, they provide better temporal resolution than chemical methods. The idea was born in 1947 when Lund & Stapp were attempting to draw an electrical current from frog skin through reversible lead/lead chloride electrodes [Lund and Rosene, 1947]. After becoming aware of the study, Hans Henriksen Ussing recalculated the currents

drawn by frog skins in terms of ion fluxes and realized that they were roughly the same order of magnitude as the net flux of sodium ions (Na^+) he had measured before. He hypothesized that the rate of active transport of ions can be measured as an electric current when an external current source is eliminating the transepithelial potential of a skin layer bathed with Ringer's solution of similar composition on both sides [Ussing, 1980]. He concluded that when the bathing solutions are identical and the potential drop across the cell layer is reduced to zero, the flux ratio for passive ions would be one, and only actively transported ions would contribute to the current passing the skin. His plans to "short-circuit" frog skins via suitable electrodes were put aside until 1950, when Ussing was assigned to give an introductory talk devoted to membrane transport problems at the 18th International Physiology Congress. As a newcomer in the ion transport field, he felt the need to justify his place in the program with some striking results. That is when he picked up his old project with only a little time left until the conference. However, in a matter of weeks, Ussing & Zerahn were able to design the chamber, wire up the circuit, and collect enough data to confirm that the net sodium flux attributes to the current drawn by the skin [Ussing and Zerahn, 1951]. In the early 1980s, the ionic conductance of the BBB of a live frog was successfully measured by Crone and his colleagues according to the theory for leaky cables priorly used in determinations of axon membrane resistance [Crone and Christensen, 1981, Crone and Olesen, 1982]. This technique became the gold standard for TEER measurement of the brain endothelium, whereas the transwell systems in combination with STX2 electrodes became the most popular for barrier

studies. However, recent studies show the necessity to validate the data obtained from these systems.

1.6 Research aims

The human bronchial epithelial cell line, Calu-3, is widely used to assess airway epithelial function and drug permeability because of an abundant supply of cells, ease of culture, reproducibility, and robustness [Mathias et al., 2002]. Calu-3 cells seem to retain constant properties and not undergo crisis over repeated passages [Shen et al., 1994]. However, similar to the BBB models, there is a large variation of the experimental TEER values across monolayers of Calu-3, ranging from $100 \Omega\text{cm}^2$ to $2500 \Omega\text{cm}^2$ [Srinivasan et al., 2015]. A wide range of values has been reported across the literature even when the experiments are conducted under the same conditions with the same cell type and measured by the same system. Calu-3 monolayers used between passage numbers 20-40 and grown in 24-well plates achieved a mean TEER value of $1056 \pm 218 \Omega\text{cm}^2$ on day 8 and $1126 \pm 222 \Omega\text{cm}^2$ on day 16 [Mathias et al., 2002]. Much lower TEER values of $300\text{-}600 \Omega\text{cm}^2$ were reported during days 10-14 for Calu-3 cells between passage number 19-35 and grown in 12-well transwells [Foster et al., 2000]. In both cases, the cells were seeded at a density of $5 \cdot 10^5$ cells/cm² in collagen-coated transwell filters under air-interface condition, and the TEER was determined using a WPI Voltohmmeter and STX-2 electrodes. The size of the transwell is the only major differing factor between these two

experiments. Nevertheless, they yield significantly different TEER values even when being normalized to the total cell culture area.

Variations in TEER values may arise due to many factors, including the overall geometry, the electrode configuration design, the electrode position, the membrane area in contact with the conducting medium, and the finite values of material's electrical properties. The normalization formula is thought to be another source of error since it assumes a homogeneous electrical field across the cell culture area, which is not the case in most of the currently used *in vitro* platforms for TEER acquisition. Moreover, the transport of the cell culture from the incubator to room conditions during measurements can cause vibrations, as well as vary the temperature and ion concentration of the conducting medium making the blank subtraction method shown by eq. 2 prone to error [Srinivasan et al., 2015]. In this thesis, it is hypothesized that differences between measurements may stem from specific measurement-related effects, such as microchannel dimensions, penetration depth of the electrodes and medium conductivity, rather than having a biological origin.

The purpose of the study is to create mapping or correction functions for a more accurate representation of the TEER values. A thorough interpretation of these values is required to allow comparisons across different *in vitro* platforms and measuring systems, as well as to quantify the effects of measurement apparatus on the accuracy of the TEER estimates. First, errors of non-biological origin contributing to differences in TEER values in transwells

and two microchip designs were identified in Chapter 2 through numerical simulations in COMSOL Multiphysics® simulation software. The theoretical data was validated through an in-house microfluidic chip in Chapter 3. Moreover, the geometrical and electrical parameter ranges of the microchip model were presented, and these parameters were ranked based on their influence on the electrical resistance response according to two well recognized sensitivity analysis methods. Chapter 4 provides a discussion of our findings.

Chapter 2

COMSOL simulations of sensitivity distribution in *in vitro* models

2.1 Introduction

Reported TEER values of *in vitro* models across the literature significantly vary even when they are obtained with the same cell type and conditions. Previous numerical simulations of transwell insert and microfluidic chip models have shown the importance of considering the entire geometry, the electrode configuration design, and the membrane properties for quantifying the TEER of a cell monolayer [Yeste et al., 2016]. The same study suggests using a weighted area based on the local contribution instead of using the total cell culture area for normalization. As abovementioned, the measured resistance is usually multiplied by the total area to obtain the TEER value for comparison between different studies. A uniformly distributed electrical field is assumed through the cell

culture. It is hypothesized that a proper interpretation and comparison of TEER values across different *in vitro* platforms can be achieved by developing a correction or mapping function for a more reliable estimation of the TEER value.

Errors in TEER measurement are presumed to arise from the use of many different measurement systems, especially when it comes to innovative microfluidic cell cultures. In the study, FEMs of the traditional transwell platform in different sizes, a microfluidic model by van der Helm et al., and an in-house microchip used for TEER acquisition were analyzed to develop a correction function for these systems. The transwell model consists of the cell culture inserts and STX2 electrodes. The microfluidic models have two main microchannels perpendicular to each other with the cell support positioned in between the cross-section of the two main microchannels (Fig. 2.1). There are four electrodes integrated into the microchannels on each side of the membrane. For initial simulations, the cell type and confluency, the temperature, the membrane porosity, the material, quality, and surface state of the electrodes, as well as electrical conductivity of the materials were assumed to be constant. It was further assumed that the electrodes were placed at the exact same position every time, there were no gaps in the cell monolayer, and the dimensions and layout of the microchips remained consistent.

The cell layer conductivity and the microchannel height were the only independent variables. The objective was to assess the current distribution of transwell inserts of different size and a microfluidic chip model of different channel heights using electrical

simulation methods, and to determine the weighted area based on the region contribution of the cell barrier. It is already well known that electrical resistance measurements conducted with STX2 electrodes in transwells with a diameter of 24 mm or larger should not be normalized to the area. In most cases, the multiplication of the resistance by the total membrane area is inaccurate [Srinivasan et al., 2015]. Since the STX2 electrodes are manually positioned, the errors associated with a change in electrode positions between measurements may also explain the dispersion of TEER values. These errors were quantified to evaluate to what degree they account for variations of TEER values in transwell insert models. The hypothesis is that TEER values are generally either under- or over-estimated based on the current distribution in the measuring platform.

2.1.1 Literature review

Previous FEMs of transwell inserts of increasing membrane area (from 24-, 12-, 6-well plates) have shown the dependence of TEER measurements on the configuration of the electrodes, the dimensions, the layout, and the type of membrane and its housing [Khire et al., 2018]. These experiments were conducted without cellular layers to avoid any variability induced by the cells. COMSOL electrical simulations demonstrate that the STX2 electrodes introduce an electric potential drop across the membrane, and consequently the non-uniformity of the electric field causes non-ohmic electrical responses. The average path taken by the charge-carrying particles from the transmitting electrodes

to the receiving ones increases in a non-linear fashion with the increasing size of the transwell [Khire et al., 2018]. The changes in path length accounting for the theoretical increase in resistance values cannot be analytically inferred because of the complexity of the geometry. This study displays the need for numerical simulations to rigorously interpret the TEER values obtained by the gold standard for measuring TEER in transwell, the STX2 electrode configuration, especially when comparing these values between different systems.

Another numerical study on the comparison of four tetrapolar electrode configurations used for TEER measurements either in transwell or microfluidic cell cultures validates these results [Yeste et al., 2016]. The STX2 electrodes, an electrode configuration with interdigitated electrodes, and two electrode configurations with integrated electrodes in microfluidic systems were studied. Based on the sensitivity distribution along the cell culture area, a geometric correction factor (GCF) was introduced as a coefficient for TEER calculation instead of the total culture area [Yeste et al., 2016]. It was found once more that a calculation error may be causing part of the dispersion of TEER values reported in the literature.

More sophisticated microfluidic systems that allow for development and customization of the device to meet specific research requirements recently emerged [Srinivasan et al., 2015]. The normalization formula has become the norm for comparisons between TEER values across the literature. There are very few papers that have validated their results through

numerical simulations. Relatively little to no attention is paid to verify the uniformity of the current density through the cell culture area.

2.1.2 Theoretical background

The COMSOL Multiphysics® simulation software was chosen over other simulation systems, such as MATLAB or Ansys Fluent, for its ease of use. Physics descriptions, associated equations, and expressions are available in the *User Interface* for customization. The *Application Builder* is also included in the software for building very specific simulation applications. The solution to the partial differential equations in the FEM model depends on the problem definition, which consists of modeling geometry, material properties, boundary conditions, governing equations, and meshing. Moreover, the number, density, and distribution of finite elements in each region, the number of element types and degrees of freedom, the coupling routines between regions described by different partial differential equations, and the numerical errors, need to also be considered to validate the numerical solution and to allow for comparisons between models. It is also important to choose an appropriate time step size for dynamic problems. Finally, the model must be experimentally validated. The accuracy of the FEM model depends on how closely the aspects of problem description match reality.

2.2 Methodology

2.2.1 Model definition

The geometric models of the transwell system and microfluidic chip were created with the AC/DC module in COMSOL Multiphysics version 6.0 using suitable 2D axisymmetric and 3D models (Fig. 2.1). The dimensions of transwell inserts of diameter 6.5 mm, 12 mm, and 24 mm (from 24-, 12- and 6- well plates, respectively) were obtained by measurements and nominal values found online. The input parameters for the geometry are shown in Table 2.2. The model geometry of the microchip, consisting of a porous membrane sandwiched at the intersection of two microchannels, was based on the design defined by van der Helm et al. However, the angles of the subchannels differ. A schematic of the transwell models, the microfluidic system by van der Helm, and our in-house microchip are shown in Figure 2.1. The microfluidic chips have four electrodes integrated into the top and bottom channels on each side of the porous membrane. The microchannels in the chip were assigned to have the same length, width, and height throughout, and the electrodes were positioned symmetrically into the model. The penetration depth of the electrodes was also assumed to be the same between the four electrodes.

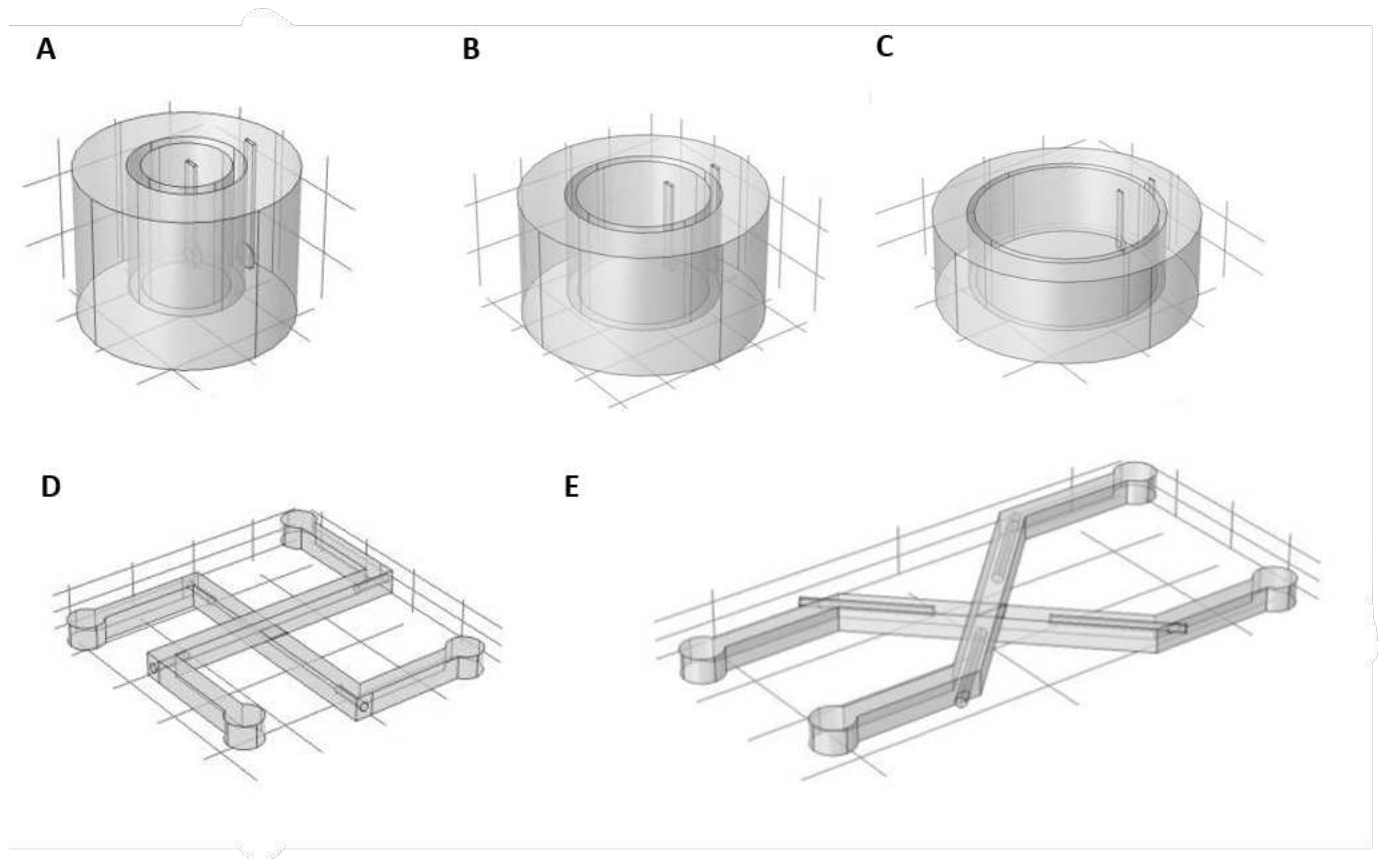


Figure 2.1: Schematics of the 3D model simulation design for A) 24-well plate transwell with insert diameter of 6.5 mm B) 12-well plate transwell with insert diameter of 12 mm C) 6-well plate transwell with insert diameter of 24 mm D) microfluidic chip designed by [van der Helm et al., 2016] E) in-house microfluidic chip

Parameter	Value	Description
$r_{24\text{-well}}$	3.25 mm	Inner radius of 24-well transwell insert
$R_{24\text{-well}}$	8.1 mm	Outer radius of 24-well transwell plate
$r_{12\text{-well}}$	6 mm	Inner radius of 12-well transwell insert
$R_{12\text{-well}}$	11.2 mm	Outer radius of 12-well transwell plate
$r_{6\text{-well}}$	12 mm	Inner radius of 6-well transwell insert
$R_{6\text{-well}}$	17.5 mm	Outer radius of 6-well transwell plate
h_f	8.4 μm	Height of transwell filter
w_{ch}	0.5 mm	Width of the top and bottom channel
h_{ch}	0.475 mm	Height of the top and bottom channel
l_{ch}	8 mm	Length of overlapping channels
l_e	1.5 mm	Penetration depth of the electrodes
d_e	5 mm	Distance between two co-planar electrodes
w_{nch}	0.5 mm	Width of the new microchip channels
h_{nch}	0.475 mm	Height of the new microchip channels
l_{nch}	8 mm	Length of overlapping channels for new chip
l_{ne}	1 mm	Penetration depth of the electrodes in the new chip
d_{ne}	6 mm	Distance between two co-planar electrodes
h_m	12 μm	Height of membrane for both models
P_m	0.3 %	Porosity of membrane
h_{cb}	30 μm	Height of cell barrier for all models

Table 2.1: Geometrical input parameters for electrical simulations.

2.2.2 Modeling considerations

The model consisted of four materials: platinum or silver/silver chloride electrodes, cell medium, porous membrane, and the cell barrier (Fig. 2.2A). The values for the conductivity and relative permittivity of Pt, Ag, and cell medium were assigned to be the same as those previously published in the literature. The conductivity of the medium was verified to be 1.54 S/m by measuring using conductivity probes. The conductivity of the semipermeable membrane was estimated by multiplying its porosity and the cell medium conductivity based on the superposition principle. Our 0.3% porosity membrane was modeled as a layer with conductivity of $0.003 \cdot 1.54 \text{ S/m} = 0.00462 \text{ S/m}$. The height of the membrane was 12 μm . The influence of the resistance of the porous membrane was generally neglected. Based on the size of ciliated cells (20-60 μm tall) previously reported [Florea et al., 2003], the cell barrier height, h_{cb} , was set to be 30 μm for a monolayer. The electrical conductivity of the cell layer was calculated based on the theoretical TEER value, Ξ_t . The theoretical TEER value was first converted to theoretical resistance, R_t by dividing it by the area in cm^2 . The cell barrier conductivity, σ_{cb} , was estimated using eq. 6 to approximate the resistance of a cell barrier of area, A_{cb} , and height, h_{cb} in a medium-filled channel using

$$\sigma_{cb} = \frac{h_{cb}}{R_t \cdot A_{cb}}. \quad (\text{Eq. 7})$$

The cell conductivities for 15 values of TEER ranging from 0-1000 Ωcm^2 were calculated. The height of the channels in the microchips was varied to study its influence on the estimated resistance value. The permittivity of the cell barrier, ε_{cb} , was found to be $2.71 \cdot 10^7$ based on the capacitance formula,

$$\varepsilon_{cb} = \frac{C_{cb}}{h_{cb} \cdot A_{cb}}. \quad (\text{Eq. 8})$$

The capacitance of the apical cell membrane, C_{cb} , is reported to be approximately 2 $\mu\text{F}/\text{cm}^2$. The relative permittivity, ε_r was calculated by dividing ε and the permittivity on vacuum, ε_0 ($8.85 \cdot 10^{-14}$ F/cm²).

2.2.3 Mesh refinement

The model was solved on progressively finer meshes with a number of nodes ranging from $1 \cdot 10^6$ to $8 \cdot 10^6$. The results were compared to choose the most accurate representation of the geometry and the solution while limiting excessive computational resources. The strategies taken to performing the mesh refinement study included using the default *physics-controlled mesh* settings to create meshes of different *element size* and using the *adaptive mesh refinement* for different adaption methods. During the adaptive mesh refinement, the solution was first computed on the initial mesh to estimate the regions where the error is high, such as the cell culture area. The geometry in these regions was then re-meshed with finer elements and the model was evolved on the finer mesh. Other than the adaptation

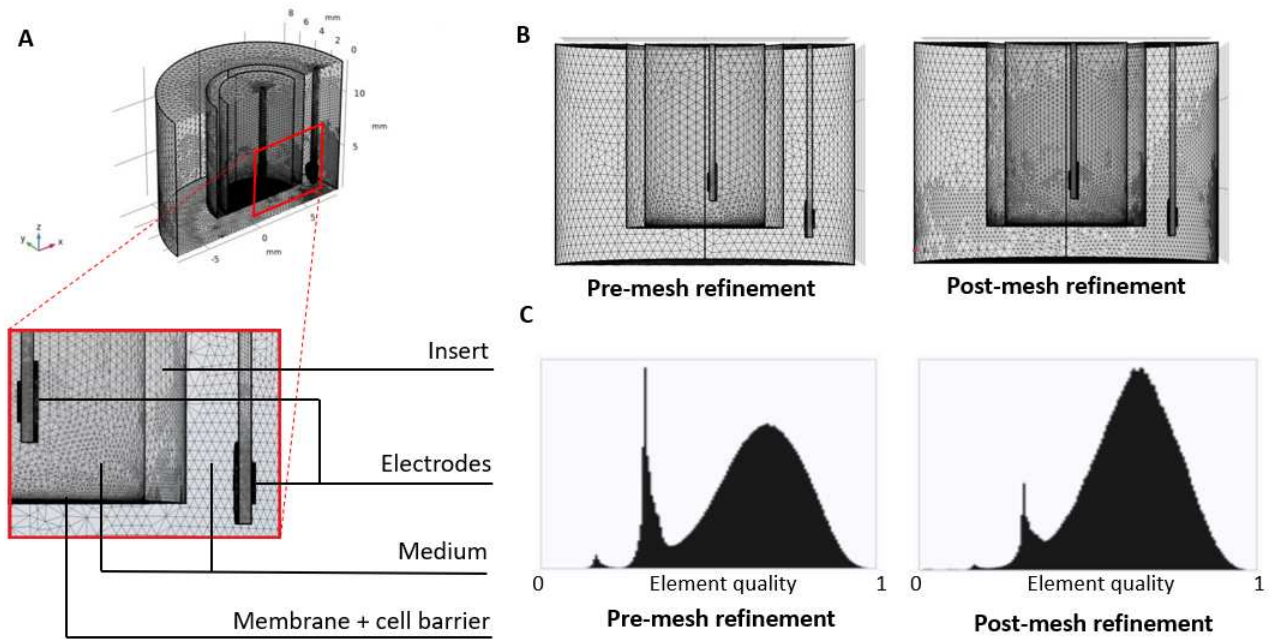


Figure 2.2: A) Cross-sectional geometrical model and mesh of the 24-well plate transwell system (insert of 6.5 mm in diameter). The simulated model mostly depends on the volume between the electrodes where the electrical current density is confined, whereas the rest of the system has a negligible effect on the measurement. B) Comparison of the mesh pre- and post-adapted mesh refinement. C) Element quality histogram for element skewedness pre- and post-adapted mesh refinement.

method, the levels of adaptive mesh refinement performed, the elements to be created, and the metric used for error estimation can also be adjusted. A combined data set can be created to compare statistical parameters between any two cases. Alternatively, mesh-related quantitative data for any geometric entity, quality measure or element type can be directly obtained by right-clicking on the desired mesh and selecting Statistics.

2.2.4 Simulation of electrical potential

Time-independent DC simulations were performed through the *Electrostatics* and *Electric Currents* interfaces to lower the computational complexity of the numerical simulations. Since the purpose of using an AC square wave current (customarily applied by commercially available Voltohmmeter systems) is to avoid any damage or charging effects on the cell layer and electrodes, this approximation provides a simplified alternative without affecting the accuracy of the simulation output. Both the *Electrostatics* and *Electric Currents* interfaces are found under the *AC/DV* module. The *Current Conservation* node in the interface provides the electrical potential equation, and defines the electrical conductivity and the relation between the electrical displacement field and the relative permittivity of the materials. The dependent variable is the electrical potential.

In both models, one of the transmitting electrodes generated a DC current of $10 \mu\text{A}$, whereas the other one is connected to the ground. The readout electrodes were set as floating potential and zero charge. All the other outer boundaries were defined to be electrical insulators. These physics features were selected from the *Physics* toolbar. A set of linear equations is derived based on Ohm's law and Kirchhoff's current law for the mesh nodes connected by the model elements. The potential in each node was calculated using the system of equations, the input current value and the conductivities of the model elements. The *Parametric Sweep* study was used to solve several variations of the model for different

values of electrical conductivity of the cell barrier and of the height of the microchannels without having to manually change the property value and re-solve each time. The *terminal resistance* (comp.ec.R11) was added as a variable by right-clicking *Global Definitions* and choosing it under Electric Currents from the context menu.

2.2.5 Sensitivity field distribution

The sensitivity of a sub-volume dv within the cell culture zone is a measure of the contribution of this volume to the measured impedance given that electrical properties like resistivity are uniform within the material. The sensitivity S was calculated as

$$S = \frac{J_1 J_2}{I^2}, \quad (\text{Eq. 9})$$

where J_1 is the current density of each sub-volume element within the material resulting from the applied current, I , across the two transmitting electrodes, whereas J_2 is the current density for the same applied current across the voltage-receiving electrodes. A positive value for the sensitivity means that an increase of the resistivity of the sub-volume elements results in the overestimation of the measured resistance. Zones with greater sensitivity values have more influence on the total resistance. Otherwise, a negative value means that increased sensitivity results on underestimation of the measured resistance. Under linear conditions, the transmitting electrodes and voltage receiving electrodes must be interchanged with no difference in measured values.

2.2.6 Geometric correction factor evaluation

The error of the TEER measurement was calculated as reported by Yeste et al. by finding the percentage difference between the simulated TEER value, Ξ_s and theoretical TEER, Ξ_t using

$$error[\%] = \frac{\Xi_s - \Xi_t}{\Xi_t} \cdot 100. \quad (\text{Eq. 10})$$

The authors proposed the inclusion of a geometric correction factor (GCF) value in the TEER calculation to account for this error in cases when part of the cell culture area contributes to the measurement. The ratio of Ξ_t to Ξ_s gives us the GCF for a system,

$$GCF = \frac{\Xi_t}{\Xi_s}. \quad (\text{Eq. 11})$$

The corrected value of TEER, Ξ_{GCF} , which accounts for the non-uniformity of the electrical field is expressed as

$$\Xi_{GCF} = (R - R_{blank})A \cdot GCF. \quad (\text{Eq. 12})$$

2.3 Results and discussion

2.3.1 Mesh Refinement

A plot of the mesh was first obtained to identify location of elements of poor quality and areas where mesh refinements are needed. Average and minimum element quality were the metrics used to evaluate mesh quality. Poor-quality elements may be tolerated when they are positioned in regions of lower density. Low-quality elements located in a critical part can lead to convergence problems. For example, in the case of the 24-well plate model, the *extra fine* mesh was selected from the default *physics-controlled mesh* settings for our 24-well plate model. The mesh generation software indicated that a face edge is too small for the chosen element size. After locating the element and deciding on their importance, we chose to perform an adapted mesh refinement. Thus, a finer mesh conforming to the previously chosen size expression was created using the *regular refinement* method. Following mesh adaptation, the elements close to the cell barrier and electrodes seem to be discretized into even several smaller elements of the same type increasing the average element quality and returning less elements of low quality (Fig. 2.2BC). In the 24-well plate transwell, the mesh included $\approx 3.39 \cdot 10^6$ elements with $\approx 9.11 \cdot 10^6$ degrees of freedom (DOFs) and $\approx 13.57 \cdot 10^6$ internal DOFs using the extra fine mesh, while the refined mesh included $\approx 10.75 \cdot 10^6$ elements with $\approx 28.98 \cdot 10^6$ DOFs and $\approx 43.00 \cdot 10^6$ DOFs. The training time lasted from a few minutes to half an hour. The created mesh was used to obtain mesh statistics. The

element quality histogram for element skewness found on the statistics window for the two meshes of the 24-well plate transwell is shown in Figure 2.2C. A quality of 1 is the best possible measure, whereas 0 represents a degenerated element. It is not possible to avoid all low-quality elements especially for geometries involving thin regions, and small edges and faces.

2.3.2 Sensitivity distribution

To determine the contribution of each sub-volume of the cell barrier to the measured resistance, the sensitivity distribution was evaluated using the Electric Currents interface on COMSOL. The optimal sensitivity should be consistent throughout and equal to unity. However, not all the sub-volumes of the cell culture region contribute equally to the final resistance when measuring TEER (Fig. 2.3). The sensitivity distribution along the cell barrier was measured on COMSOL for different systems and TEER values.

The introduction of the STX2 electrodes highly impacts the sensitivity field in the transwell model. It was found that zones between and close to the electrodes contribute more than the zones far from them. Sensitivity profiles reveal maxima close to or below the electrodes, and minima around the center of the cell culture area. The microfluidic chip models, B and C, display a more uniform sensitivity field than model A. Both microfluidic models present large differences between the sensitivity of zones of the cell culture area, especially at the ends of the microchannels. The differences are lower at the center. For the

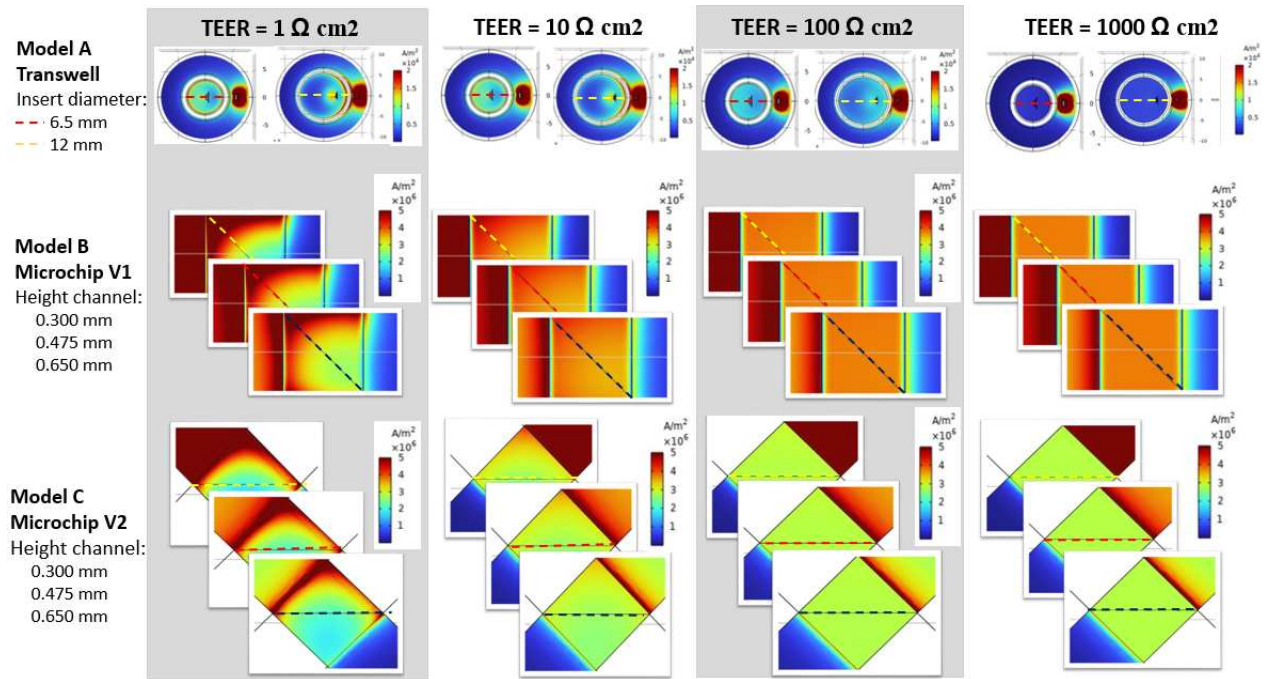


Figure 2.3: Current density norm $[A/m^2]$ along the cell culture area shown in 2D sections when TEER is obtained in a transwell culture insert using STX2 electrodes (model A), in a microfluidic model of van der Helm et al. (model B), and our in-house microchip model (model C). Results are presented for different insert diameters (6.5 mm and 12 mm) and different channel heights (0.300, 0.475, and 0.650 mm) for TEER equal to a) 1 Ωcm^2 b) 10 Ωcm^2 c) 100 Ωcm^2 d) 1000 Ωcm^2 .

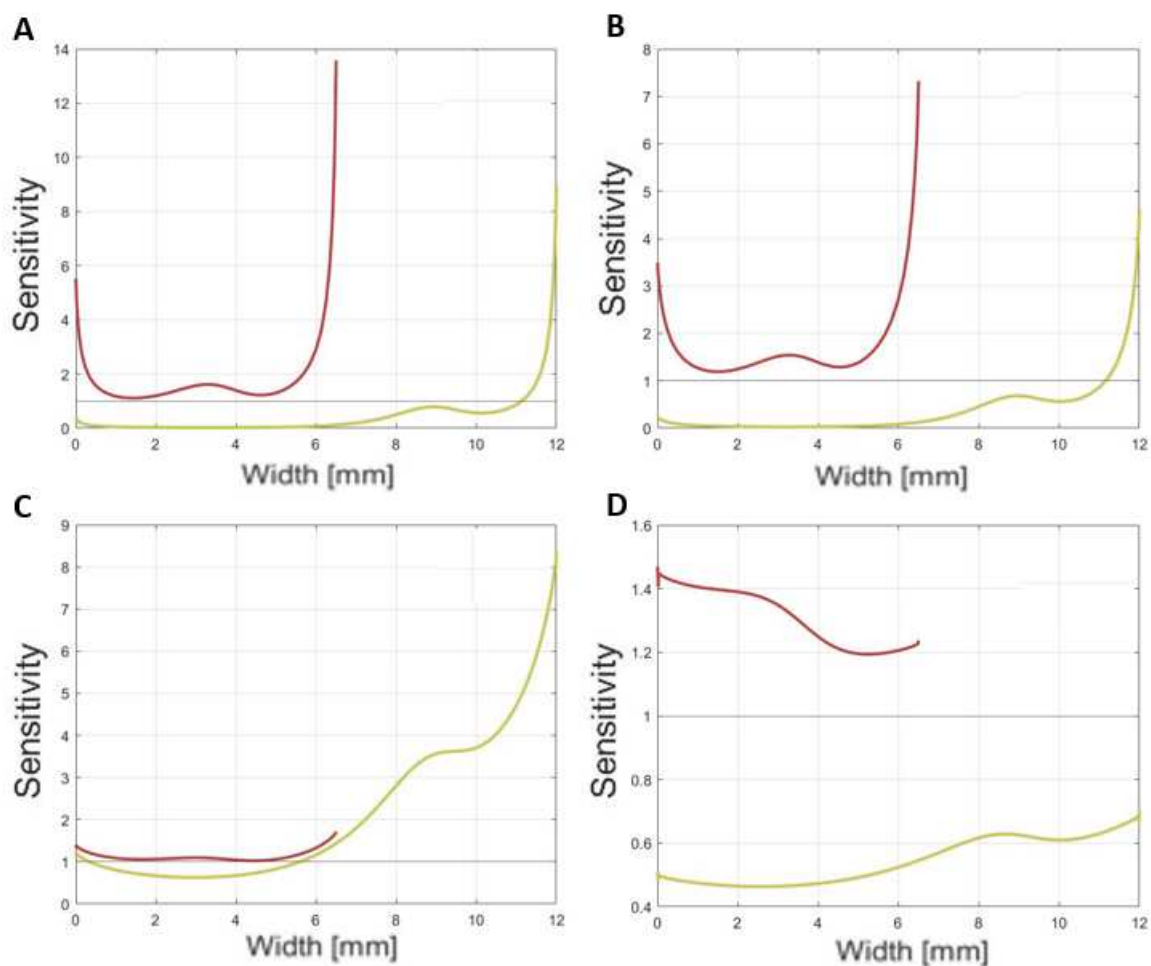


Figure 2.4: Sensitivity profile of the cell barrier along the dashed line axis shown in Fig. 2.3 in a transwell culture insert using STX2 electrodes (model A). Results are presented for different insert diameters (6.5 mm in red and 12 mm in yellow) and TEER values: A) 1 Ωcm^2 B) 10 Ωcm^2 C) 100 Ωcm^2 D) 1000 Ωcm^2 .

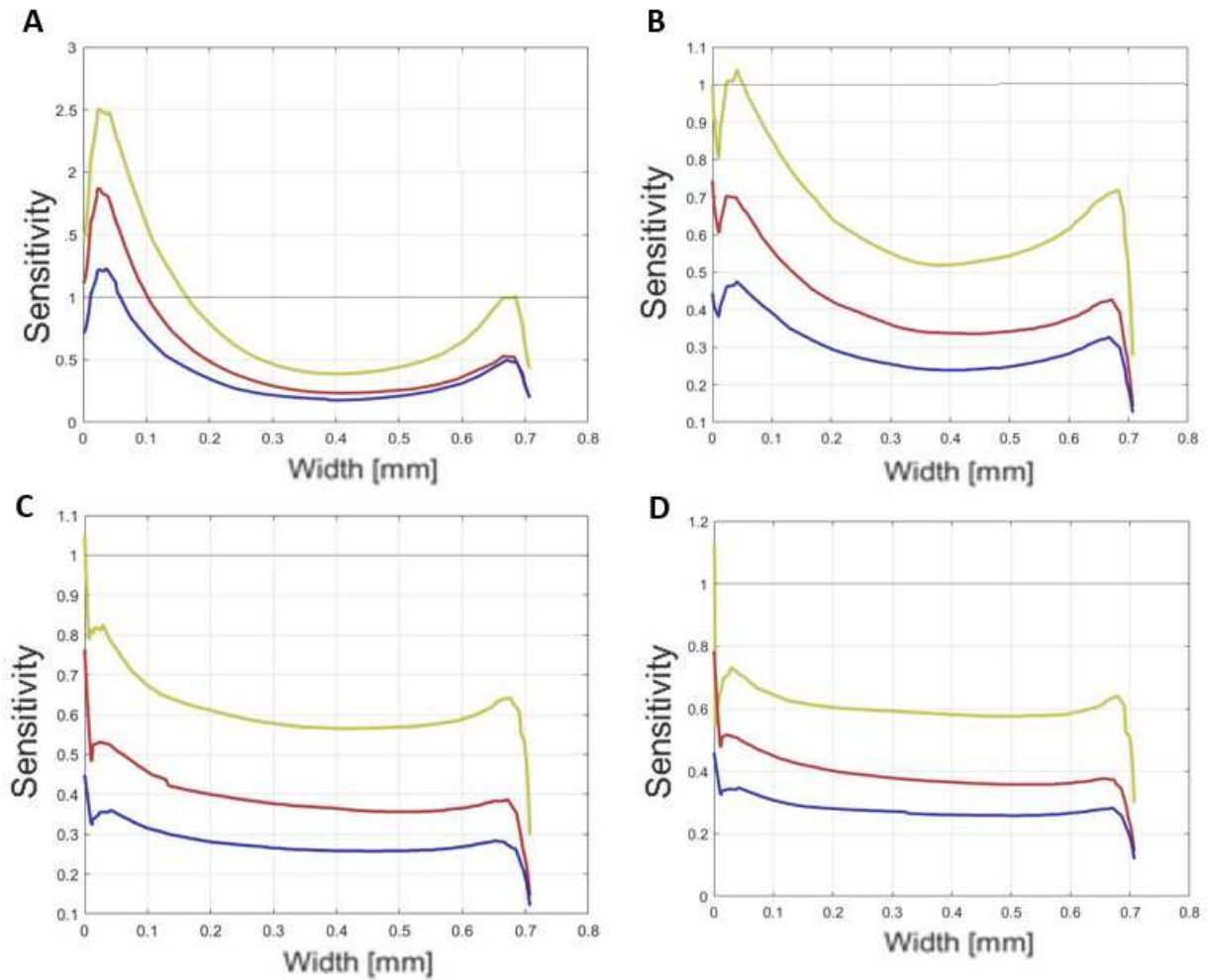


Figure 2.5: Sensitivity profile of the cell barrier along the dashed line axis shown in Fig. 2.3 in a microfluidic model as designed by van der Helm et al. (model B). Results are presented for different channel heights (0.300mm in yellow, 0.475 mm in red, and 0.650 mm in blue) and TEER values: A) $1 \Omega\text{cm}^2$ B) $10 \Omega\text{cm}^2$ C) $100 \Omega\text{cm}^2$ D) $1000 \Omega\text{cm}^2$.

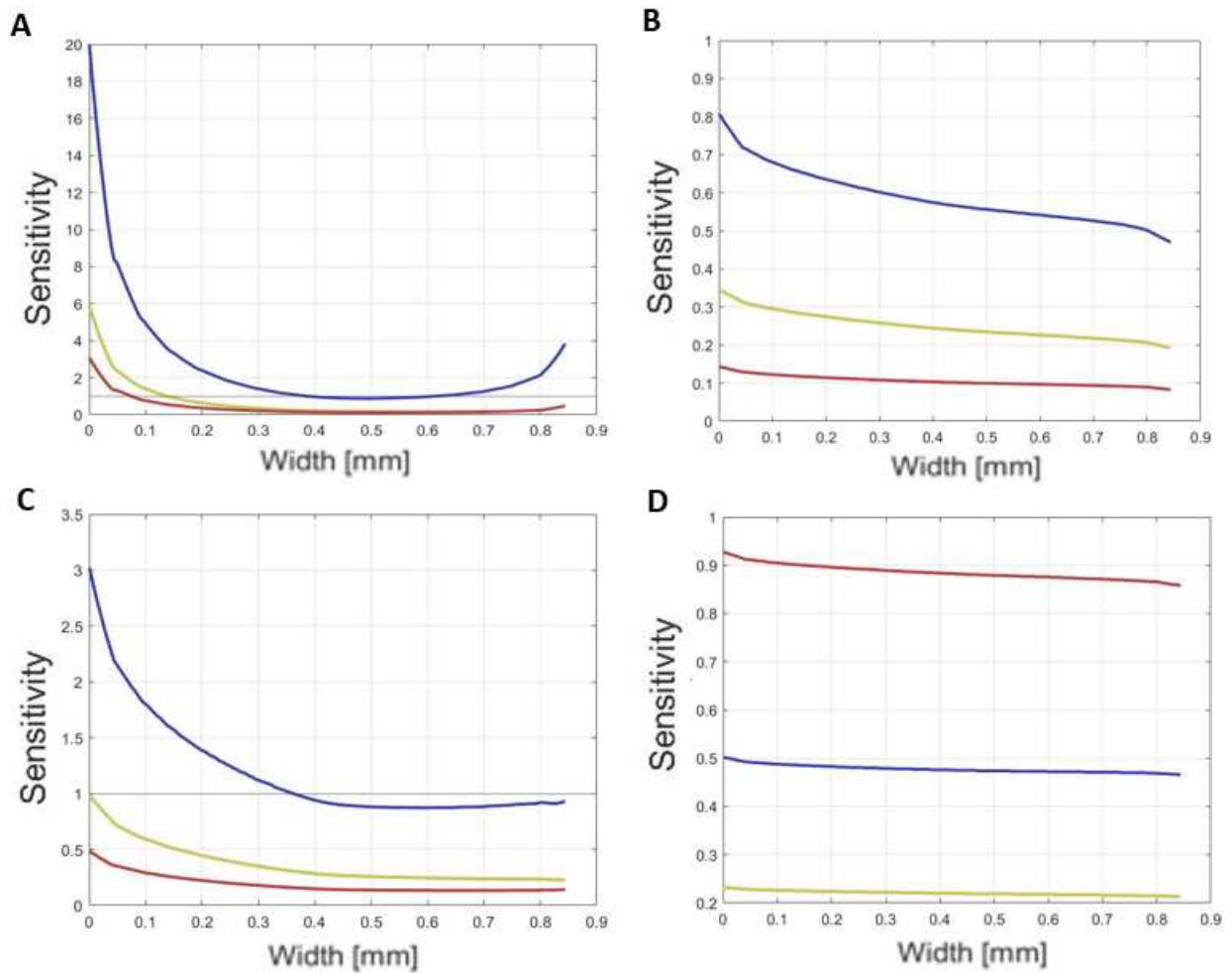


Figure 2.6: Sensitivity profile of the cell barrier along the dashed line axis shown in Fig. 2.3 in our in-house microchip model (model C). Results are presented for different channel heights (0.300mm in yellow, 0.475 mm in red, and 0.650 mm in blue) and TEER values: A) 1 Ωcm^2 B) 10 Ωcm^2 C) 100 Ωcm^2 D) 1000 Ωcm^2 .

most part, model C displays better uniformity for the sensitivity field than model B, especially when it comes to TEER values greater than $100 \Omega\text{cm}^2$. In fact, the uniformity of the sensitivity field generally increases with TEER. For TEER values greater than $1000 \Omega\text{cm}^2$, sensitivity variations are less than 4% for model C, and less than 16% for the transwell inserts (Fig. 2.6; Fig 2.4). On the other hand, model B has distinct sensitivity peaks near the microchannels, but a rather uniform deficit in the center of the cell culture area.

The microchannel geometry is another feature that highly affects the sensitivity. The field discontinuities displayed in Figure 2.5 and 2.6 are due to the high resistance of the small channels. Narrow channels limit current flow in areas of the cell barrier that are far from the electrodes. The most uniform sensitivity is achieved for larger channel heights in model B. It seems to be lower for bigger channels, model C. The reason behind this may be the closer positioning of the electrodes to one another in the second model. A ranking of the model parameters were determined and is shown in the next Chapter.

2.3.3 Geometric correction factor

Incorrect calculations for TEER may be due to the use of eq. 3 to normalize the resistance to the total area while wrongly assuming a uniform sensitivity field. The issue can be solved by using eq. 12 which includes a GCF. The GCF would be close to unity when there is no error in TEER calculation using eq. 3, and away from unity when there

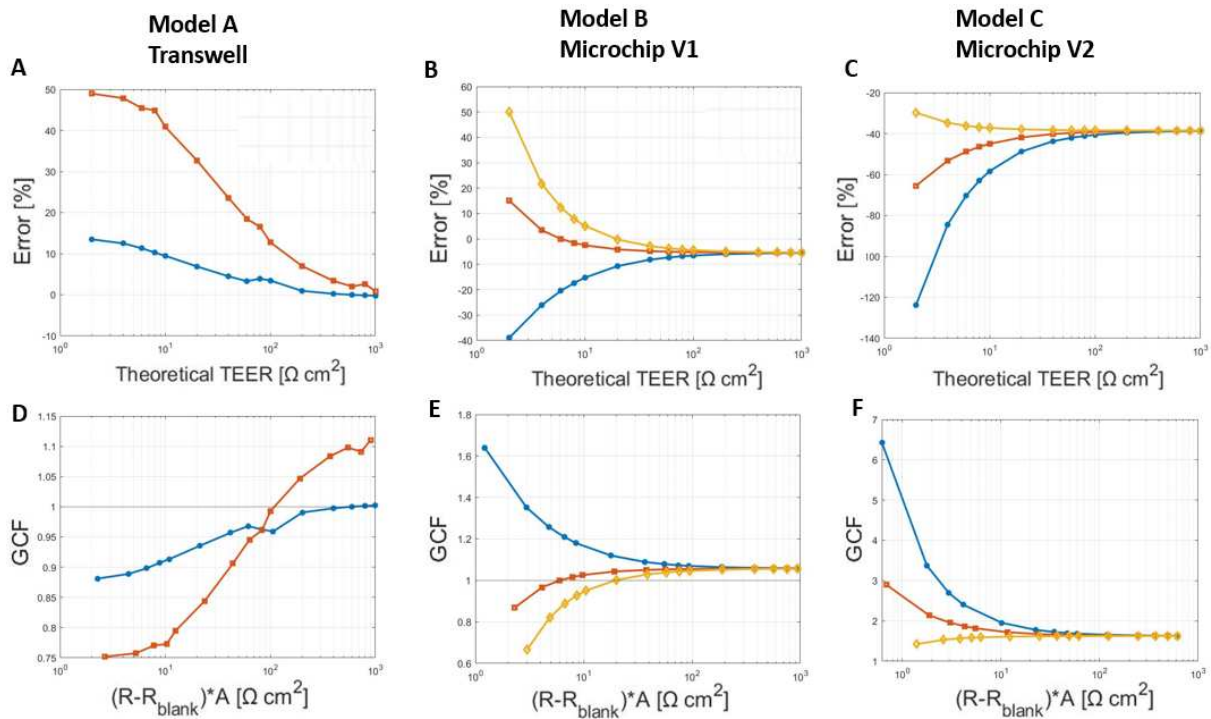


Figure 2.7: A) B) C) Error [%] and D) E) F) GCF when TEER is obtained in a transwell insert of diameter 6.5 and 12 mm (model A) and in the microfluidic models (model B & C) for different microchannel heights (0.300mm in yellow, 0.475mm in red, and 0.650 mm in blue).

is a significant error. The geometric error associated with each system and the GCF value to be used in the TEER calculation for different simulated models is shown on Figure 2.5. In general, there is less error associated with higher values of TEER (Fig. 2.7). There is a measurement error of $\approx 5\%$ for model A and B, and $\approx 39\%$ for model C when the cell conductivity of the cell layer is 0.0003S/m which corresponds to a theoretical value of $1000\ \Omega\text{cm}^2$. The percentage errors are for the most part higher for lower TEER values of the cell barrier. In all models, the GCF is close to unity for a TEER of $1000\ \Omega\text{cm}^2$, while it varies for lower values (Fig. 2.7). The results agree with those from the sensitivity distribution section. A GCF lower than unity found in models B and C, is associated with an overestimation of the value, whereas a GCF higher than unity indicates an underestimation.

While it is already advised that transwell inserts of 24 mm or larger in diameter should not be normalized to the area, it has been shown that even measurements with inserts of 12 mm in diameter are not very accurate and require a GCF [Yeste et al., 2016]. Concerning the microfluidic systems, the microchannel height also highly affects the GCF value. Thus, it is important to consider the dimensions, the layout, and the size and placement of the electrodes when designing systems used for TEER acquisition.

2.3.4 Influence of electrode placement on TEER values in transwells

The STX2 electrodes must be repeatedly positioned into the system. The sensitivity field is highly affected by their introduction into the insert. The sensitivity is not uniformly distributed with zones close to the electrode having a much higher contribution to the resistance to those far away. The non-reproducibility placement of the STX2 electrodes accounts for variations of TEER. The errors associated with positioning the electrodes at different locations in the transwell was studied by simulating the resistance of a model with a cell barrier at an electrical conductivity of 0.003 S/m, which corresponds to a theoretical TEER value of 100 Ωcm^2 . The resistance of the cell barrier in 6-, 12- and 24-well inserts was simulated for spatial variations of 1 mm from the central position of the electrodes. Given that the electrodes are always located parallel to the insert plate, the user can still end up varying their position during reinsertion. There was a 2.4% fluctuation in value for 24-well plates which have the smallest diameter and the most uniform sensitivity distribution. However, a spatial variation of only 1 mm can alter the TEER values by approximately 6.9% for both the 6- and 12-well transwell plates. Thus, the STX2 electrodes must be carefully placed to allow recurred measurements. It is highly recommended to use a system that automates their placement in transwell inserts, such as the REMS AutoSampler from WPI Inc.

Chapter 3

Experimental validation and parameter ranking

3.1 Background

The factors that influence the current distribution include the shape of the cell culture, the physics of the surrounding micro-environment, the electrode configuration, as well as the changing electrical conductivity of the cell layer. Other than differences resulting from variations across microfluidic models, the final microfluidic chip geometry is also variable. Additionally, uncertainty in geometric and electrical parameters may contribute to overall model errors. Previous studies involving numerical simulations of TEER measurement in transwell inserts and microfluidic models have used estimates for most parameter inputs [Yeste et al., 2016, Khire et al., 2018, Helm et al., 2019]. In most cases, the same material parameter estimates end up being used repeatedly. For example, a single estimate of the medium electrical conductivity was used across at least three independent studies. Considering that the temperature and the composition of the medium

can considerably affect its conductivity, it is very unlikely that this parameter has a unique value. For convenience, the same values are used for comparisons between different studies.

The purpose of the present study was to investigate the electrical resistance response of a microfluidic chip model to a constant applied current across a broad range of model parameters. The design of the sub-channels was altered from a previous design by van der Helm et al. [2016]. Based on stochastic modeling, simulation models can predict parameter outputs that account for certain levels of unpredictability or randomness. The aim is to identify and rank the model parameters from the least to the most sensitive to later optimize the final design of our microfluidic chip. The general hypothesis is that TEER values obtained from *in vitro* models are either insensitive, moderately sensitive, or highly sensitive to certain model parameters. The modeling forecast can provide valuable information to optimize the values of these parameters, design more accurate and efficient systems in future studies, and minimize uncertainty during measurements.

Our microfluidic model was experimentally validated by running experiments on the in-house microfluidic chip (Fig. 2.1E). The resistance of the polyester membrane was measured for different penetration depths of the electrodes into the microfluidic channels. The final length of the electrode in touch with the medium was later measured by microCT scanning to compare the simulated data with our empirical values.

3.2 Methodology

3.2.1 Mold 3D printing

The mold with the channel designs was created on Solidworks CAD software and printed by a Formlabs SLA 3D printer (Form 2) with a maximum resolution of $\approx 100 \mu\text{m}$. The material was a light-curable polymer chosen for its biocompatibility, high-impact strength, water resistance, and sterilization compatibility. After printing, the part was rinsed with isopropyl alcohol (IPA) $\geq 99\%$, washed for 15 min, and soaked for another 5 min in fresh IPA. After verifying that the parts were clean and dry, with no residual alcohol, liquid resin or residues remained on the surface, the part was post-cured at 60°C for 60 minutes.

3.2.2 Fabrication of the organ-on-chip device

The protocol for microchip fabrication was adapted from van der Helm et al. [2016]. Polydimethylsiloxane (PDMS) base and curing agent (Sylgard 184 Silicone elastomer kit, Dow Corning) were mixed in a 10:1 mass ratio. After thorough mixing, the solution was degassed in a desiccator for ≈ 30 min to remove the air bubbles. The mixture was then poured into a 3D-printed mold and cured in an oven at 60°C for 4 hours. The cured PDMS with channel imprints was later cut into separate top and bottom parts. Using a sharp biopsy punch (1 mm in diameter), four holes were punched inside out in the top part to form the inlets. The parts were covered by clear tape to protect them from dust. To create the

leakage-free PDMS ‘mortar’ layer, PDMS base agent, PDMS curing agent and toluene were vortexed thoroughly with a 10:1:6 weight ratio. The mixture was allowed to settle at room temperature for ≈ 5 min to remove the air bubbles. To obtain a thin and uniform mortar layer, the prepolymer was transferred to both PDMS halves using a thin paintbrush. The polyester membrane with $0.4 \mu\text{m}$ pores and $12 \mu\text{m}$ thickness (Polyester PETE membrane filters, transparent; Sterlitech Corporation) was cut into small squares of 9 mm^2 surface area. The edges of the porous membrane were manipulated using a set of tweezers and dipped into the mortar before being placed in the center of the bottom PDMS part. The top half was carefully aligned and placed on the bottom half without applying pressure to prevent the mortar from clogging the membrane and entering the channels. Alternatively, the PDMS and membrane substrates were exposed to an oxygen plasma for 2 mins at 100 W. Pressure was applied for 5 mins until adhesion. The chips were later covered with clear tape and baked for three hours at 60°C . Lastly, four platinum (Pt) electrode wires ($250 \mu\text{m}$ diameter; Thermo Scientific(TM)) were deposited into the electrode channels on each side of the microchip by UV glue and defined by UV exposure. Micro-CT scanning was used to confirm the size of the channels and the position of the electrodes after building the model. After rinsing with PBS, the microchannels were filled with medium at room-temperature. The TEER measurements were conducted with an EVOM device connected to a telephone cable and Pt electrodes. We attempted to keep the electrode position consistent in all five samples. Experiments were done without cell monolayers to avoid any cell-induced variability.

3.2.3 Modeling Considerations

The geometry, boundary conditions, and certain parameter values were identical to those described in Chapter 2. The microchannels were assumed to have a constant width and length throughout. Parameter ranges were chosen instead of parameter values for the microchannel height, h_r , microchannel width, w_r , penetration depth, d_r , as well as for the conductivity of the media, σ_{r-m} , and of the cell barrier, σ_{r-cb} . The media's electrical conductivity is reported to vary from 1.5 to 1.7 S/m [Lang et al., 2015]. Since the TEER acquisition for Calu-3 cell barriers under AIC is conducted in channels filled with PBS, the electrical conductivity of 10.2 S/m was set to be the maximum of σ_{r-m} . The same range of values was chosen for σ_{r-cb} as before. The microchannel height was set to vary from 0.300 mm to 0.650 mm, the microchannel width from 0.400 mm to 0.600 mm whereas the penetration depth into the medium from 1 mm to 3 mm. The minimum height was set as 0.300 in order to allow the integration of the Pt electrode into the channel. All geometric and electrical parameters with their associated ranges are listed in Table 3.1 and Table 3.2, respectively. Hundreds of unique FEMs were created in this study using the *Parametric Sweep* function on COMSOL. The same mesh type was applied to each microchip model. Simulations of the fabricated microchips with its matching dimensions and cell culture conditions were also conducted to cautiously interpret the resulting data.

Parameter	Value	Description
C_{dl}	$20 \mu\text{F}/\text{cm}^2$	Double layer capacitance of electrodes
ε_m	78	Relative permittivity of culture medium
C_{cb}	$2 \mu\text{F}/\text{cm}^2$	Approximated capacitance of cell membrane
σ_{Ag}	$6.21 \cdot 10^9 \text{ S/m}$	Specific conductivity of Ag
σ_{Pt}	$9.43 \cdot 10^9 \text{ S/m}$	Specific conductivity of Pt
σ_m	1.54 S/m	Specific conductivity of culture medium
I	$10 \mu\text{A}$	Input current
$TEER_t$	$0\text{-}1000 \Omega\text{cm}^2$	Range of possible theoretical TEER value

Table 3.1: Electrical input parameters for electrical simulations.

Parameter	Value	Description
σ_{r-m}	$1.5\text{-}10.2 \text{ S/m}$	Range of possible electrical conductivities of the media
$TEER_{r-t}$	$0\text{-}1000 \Omega\text{cm}^2$	Range of possible theoretical TEER value
h_r	$0.300\text{-}0.650 \text{ mm}$	Microchannel height
w_r	$0.400\text{-}0.600 \text{ mm}$	Microchannel width
d_r	$1\text{-}3 \text{ mm}$	Range of penetration depths of electrodes

Table 3.2: Geometrical input parameters for electrical simulations.

3.2.4 Data analysis

The Pearson's correlation coefficient test was used to study the strength of the linear relationship between the simulated and experimental values. Two different sensitivity analysis techniques were applied to analyze the output data. The influence on overall electrical resistance, on the electrical resistance of the membrane, and on the latter normalized to the area was studied based on the selected range of parameters. First, we applied a screening method that ranks model input parameters based on their influence on the output by using a two-level fractional factorial design. The approach involves $2n+2$ simulations, which reduces the computational complexity but usually fails to precisely quantify the contribution of each parameter. Since there are five independent variables in our study, the implementation involves only 12 cases. The parameter values were set to either the high or low extremes, with case 0 consisting of all parameters set to low values, whereas intermediate cases n to $2n+1$ of one of the parameters set to an extreme and the other parameters set to the opposite extreme. For the final case, all parameters are set to high values (Table 3.3). Cases 1-5 are the reverse situation of cases 6-10.

The equation for the importance value of the j^{th} element, represented by M_j is

$$M_j = |y_{2n+1} - y_{n-j} + y_j - y_0| + |y_{2n+1} - y_{n+j} - y_j - y_0|, \quad (\text{Eq. 13})$$

where y is the output resistance for a certain case.

Case	Parameter				
	P1	P2	P3	P4	P5
0	L	L	L	L	L
1	H	L	L	L	L
2	L	H	L	L	L
3	L	L	H	L	L
4	L	L	L	H	L
5	L	L	L	L	H
6	L	H	H	H	H
7	H	L	H	H	H
8	H	H	L	H	H
9	H	H	H	L	H
10	H	H	H	H	L
11	H	H	H	H	H

Table 3.3: Cotter’s simulation cases for a five-parameter model. High and low parameter values are indicated by H and L, respectively.

A local sensitivity analysis was also performed. The local sensitivity, S , of each set of parameters, M , to each parameter, Y , is defined as the partial derivative and was evaluated by the finite difference approximation,

$$S = \frac{\delta M}{\delta Y} \approx \frac{M - M_{nom}}{(Y - Y_{nom})/R}. \quad (\text{Eq. 14})$$

The initial value of M with its associated nominal parameter value, Y_{nom} , was randomly selected. After altering parameter Y with all the other parameters kept constant, the output for M was recorded. Each parameter was non-dimensionalized by dividing the change in parameter value and the range of the parameter, R . Thus, the sensitivity can be defined as the change in resistance due to a percent change in one of the parameters. This approach

was used to obtain 872 total sensitivities for each case. The mean and standard deviation were recorded.

3.3 Results and Discussion

Model verification was achieved by comparing our experimental and numerical model analysis for different electrode positions. There is a strong correlation between the results and our simulation data since the Pearson's correlation coefficient is ≈ 0.91 . The geometric and electrical parameters for Model C were ranked according to their influence on overall resistance, R_t , resistance of the membrane, R_m , and the latter normalized to the area, $A \cdot R_m$. A mesh refinement study indicated that the selected mesh was spatially converged. The mesh consisted of $\approx 3.87 \cdot 10^6$ elements with $\approx 7.71 \cdot 10^6$ degrees of freedom (DOFs) and returned an average element quality of 0.68 for skewness.

3.3.1 Parameter ranking

The importance value statistics produced by Cotter's screening method are shown in Table 3.4 as functions of the parameters (electrical conductivity of the medium, electrical conductivity of the cell barrier grown on the membrane, channel height, channel width, and penetration depth) for all three resistances; R_t , R_m , and the latter normalized to the area, $A \cdot R_m$. Cotter's method ranked the width of the channel, w_r , as the most influential factor to the total resistance of the system, R_t , while the conductivity of the medium, σ_{r-m} , was the

Parameter	Importance value (mean \pm std [Rank])		
	R_t	R_m	$A \cdot R_m$
σ_{r-m}	27.1 \pm 14.7 [5]	51.7 \pm 7.6 [1]	45.7 \pm 13.8 [2]
σ_{r-TEER}	47.7 \pm 7.3 [2]	50.5 \pm 7.6 [3]	43.6 \pm 13.8 [4]
h_r	38.2 \pm 7.6 [4]	49.9 \pm 7.6 [4]	43.3 \pm 14.0 [5]
w_r	86.0 \pm 9.3 [1]	47.4 \pm 2.4 [5]	80.5 \pm 1.9 [1]
d_r	38.8 \pm 7.4 [3]	50.9 \pm 7.6 [2]	44.3 \pm 13.8 [3]

Table 3.4: Importance value statistics obtained from Cotter’s method. R_t refers to the total resistance, R_m to the membrane resistance, and $A \cdot R_m$ to the membrane resistance normalized to the area. The parameters consist of the conductivity of the media, σ_{r-m} , the conductivity of the cell barrier, σ_{r-cb} , the microchannel height, h_r , the microchannel width, w_r , and the penetration depth, d_r .

least influential. It should be noted that the width of the channel is associated with the area of the membrane. The area is equal to w_r^2 . After using the six measurement configuration method proposed by van der Helm et al. [2016], the parameters appear to have around the same amount of influence on the simulated resistance value of the membrane. As expected, the normalized resistance, $A \cdot R_m$, is most sensitive to the width of the membrane, while a similar consistency as before was found between the other four parameters.

A total of 8720 total local sensitivities were collected to rank the parameters based on descriptive statistics. Before normalizing the values to the area, both the overall and membrane electrical resistance were the least sensitive to the height, h_r , and the width, w_r , of the microchannels. There is an increase in the local sensitivity for w_r after the six measurement configuration calculations are carried out. The six measurement configuration calculations also make d_r and σ_{r-m} have less impact on the output, which shows that the

Parameter	Local sensitivity (mean \pm std [Rank])		
	R_t	R_m	$A \cdot R_m$
σ_{r-m}	58.2 \pm 47.1 [1]	-3.8 \pm 2.3 [1]	-5.8 \pm 3.2 [2]
σ_{r-TEER}	36.29 \pm 22.4 [3]	3.2 \pm 2.6 [3]	13.5 \pm 11.4 [1]
h_r	-2.8 \pm 4.5 [4]	-1.0 \pm 1.2 [5]	-5.3 \pm 6.2 [3]
w_r	0 [5]	1.5 \pm 1.4 [4]	3.6 \pm 3.4 [5]
d_r	-53.5 \pm 36.2 [2]	-3.6 \pm 3.4 [2]	-4.1 \pm 2.8 [4]

Table 3.5: Statistics for local sensitivity values. R_t refers to the total resistance, R_m to the membrane resistance, and $A \cdot R_m$ to the membrane resistance normalized to the area. The parameters consist of the conductivity of the media, σ_{r-m} , the conductivity of the cell barrier, σ_{r-cb} , the microchannel height, h_r , the microchannel width, w_r , and the penetration depth, d_r .

chip design does indeed reduce variability stemming from the double layer capacitance of the electrodes and the changing conditions of the medium. For both cases, the most sensitive parameters were σ_{r-m} , d_r , and σ_{r-TEER} . After normalization of the resistance to the total area, it was found that the σ_{r-TEER} and w_r have a positive correlation with the resistance, unlike σ_{r-m} , h_r , and d_r . In fact, σ_{r-TEER} becomes the most influential factor in measurements, followed by σ_{r-m} and w_r . This is in agreement with expectations. The goal is to optimize the device so the resistance values are most sensitive to the electrical conductivity of the cell barrier seeded on it.

The two methods utilized are not directly comparable, since they each incorporate different amounts of data, rely upon different assumptions and produce different rankings. Cotter's method fails to identify the key parameters and the correlations between the inputs and outputs although it requires less computational cost than the local sensitivity

analysis. Another advantage of the local sensitivity method is its ability to allow comparisons between sensitivities of different parameters, since the parameter value gets non-dimensionalised. The two methods do not agree in every respect. The cause of these discrepancies may be the unidentified interaction effects with other parameters, the sample size, or the choice of parameter ranges.

Chapter 4

Discussion and Conclusions

Few studies have discussed the source of the dispersion of TEER values across the literature. In this study, the importance of considering the sensitivity distribution while designing TEER measuring devices was demonstrated. A sensitivity field plot of the measurement apparatus was obtained using FEMs and has proven to be a very valuable tool for experimental design (Fig. 2.4). In transwells, the resistance was more sensitive to volumes close to or below the electrodes rather than volumes far from them, which leads to an in-homogeneity of the sensitivity distribution along the cell culture area (Fig. 2.4). On the other hand, the microfluidic chips were found to have a more uniform sensitivity field (Fig. 2.5; Fig. 2.6). Nevertheless, the sensitivity profile revealed an electric potential drop near the ends of the microchannels while the central part of the cell culture area displays a consistent deficit. Furthermore, there was a clear dependency of the TEER and the microchannel height on the sensitivity for all models. As the TEER value of the cell culture area increased, there were fewer sensitivity variations for all models.

The COMSOL software was also employed to create a correction function (GCF) for all systems in order to calculate the true value of TEER. Since the regions of the cell culture area do not equally contribute to the overall electrical resistance, the normalization formula used for TEER calculations is inaccurate. It is necessary to use a GCF to allow for comparisons of the values collected from different measuring systems. The errors and GCF values for specific TEER values ranging from 0 to 1000 Ωcm^2 and microchannel heights are shown in Figure 2.7. The error was defined as the percentage difference between the simulated and theoretical TEER value. When no GCF was used, the simulation models displayed high measuring errors for low TEER values and small channel heights. These errors were found to be $\approx -5\%$ for model B and $\approx 39\%$ for model C when measuring TEER values greater than 100 Ωcm^2 . The GCF got close to unity within these range of TEER values for the two microchip models.

The errors associated with electrode positioning in transwells were also quantified in this chapter. A positioning error of 1 mm was detected to cause a $\approx 6.9\%$ fluctuation in TEER values for both the 6- and 12-well transwell plates, and a $\approx 2.6\%$ fluctuation for the 24-well plate. The average path taken by the charge-carrying species increases in a non-linear fashion with increasing size of the transwell, leading to a non-uniformity of the sensitivity distribution in bigger transwells.

In Chapter 3, the model was experimentally validated by comparing the empirical and simulation data collected from the in-house microfluidic chip model measuring the

resistance of a blank membrane for different penetration depths of the electrodes. The four-terminal sensing approach used in our studies removes uncertainties stemming from the contact and lead resistances and from the double layer capacitance at the interface between two electrodes. It also provides a better optical visualization of the cell culture, which is a very useful characteristic for the development of future microfluidic systems that claim to reproduce and monitor different cell barrier functions. The results displayed a linear correlation of ≈ 0.91 between the two methods.

The Cotter's screening method and the local sensitivity analysis were used to rank five model parameters, consisting of electrical conductivity of the medium and the porous membrane, the height and the width of the microchannels, as well as the penetration depth of the electrodes. These parameters were ranked based on their influence on the overall electrical resistance, the membrane resistance, as well as on the latter one normalized to the area. Our results show that the six measurement configuration method is helpful in reducing the effects of electrodes' double layer capacitance and the conductivity of the medium on the membrane resistance as shown by both methods (Table 3.1; Table 3.2). However, the Cotter's method can provide us with misleading results, as the parameters are dimensionalized and the sample size is small. The local sensitivity method confirmed the relative influence of each parameter to the resistances. The ranking of local sensitivity values differed depending on the output parameter. For example, the membrane resistance was more sensitive to the width of the membrane, while the total resistance was insensitive

to it. On the other hand, the impact of the other four parameters on the resistance of the membrane reduced relative to their impact on the total resistance. As expected, the normalized membrane resistance was most sensitive to the conductivity of the membrane while analyzed by the local sensitivity method. The influence of the other parameters is not completely eliminated.

This work serves as a theoretical foundation to experimentally validate and adopt the use of our microfluidic chip or other measuring systems for TEER acquisition of cell barriers. Close attention must be paid to the development of novel microchip devices to achieve better accuracy for the resulting TEER value. While it may not be possible to control every variable, the conditions should be optimized and simplified to satisfy the user's needs. Moreover, it is important for laboratories to identify and report the exact conditions of cell growth and the above listed independent variables when reporting TEER values. The same values as observed under *in vivo* conditions must be reached through *in vitro* models to accurately evaluate transport of drugs or chemicals in these systems.

4.1 Limitations

Possible limitations of the numerical studies include the size of the mesh and the assumptions made during problem definition for the overall geometry, the material properties, the governing equations, and the boundary conditions. The simplified resistance model circuit used for TEER measurements in transwells and in the microfluidic chips may also lead

to erroneous results. Moreover, there are large variations in the local sensitivity statistics. This may be partially resolved by conducting more simulations to have a greater sample size or by limiting the parameter range. Lastly, during experiments, air bubbles may have blocked the effective cell culture area. A change in temperature or composition of the cell medium, or in the electrode positioning may also occur when the system is temporarily removed from the incubator. These changes may cause a dispersion of the values.

4.2 Future directions

Biological factors may greatly influence the TEER value. It has been shown that once total confluence has been established, the TEER measurement technique cannot differentiate between a tight monolayer and a thick pseudostratified layer since the TEER values reach a plateau after confluence [Bol et al., 2013]. Further numerical simulations should be analyzed to discover the impact of cell growth and morphology on the values. TEER in its own can be misleading. The impedance spectroscopy (IS) measurement method can be used to get cell capacitance information and avoid blank measurements.

A study in rat primary ATI-like yielded equivalent TEER values at day 8 under submerged and air-interface conditions (AIC), while mannitol permeability was higher under the air-interface condition [Fang et al., 2004]. On the other hand, cultured 16HBE14o- under submerged conditions yielded a six-fold higher TEER value compared to cells under AIC, which is consistent with the more intense staining of TJ proteins observed

in submerged cell cultures. The choice in cell types and growth conditions (i.e. submerged vs AIC) strongly influences the differentiation process, including the types of transporters present on the cells, and their regulation [Shen et al., 1994]. Therefore, these studies indicate that in many cases, the discrepancy between TEER values could be due to cell specific reasons. The influence of frequency on cell-specific parameter sensitivity also remains to be studied. Impedance sensing has been used for decades for tracking collective behavior of cell layers. The latter's respective signatures can become hidden when they overlap spectroscopically, and variations of the impedance values cannot be easily untangled to give out specific cellular property changes. Thus, further attempts should be made in deconvolving the impedance spectra to reveal the underlying property changes using numerical simulations.

4.3 Broader implications

Normal functioning of all the organs of our body is dependent on having intact barrier tissues. Damage or disintegration of the barrier functions in the brain, lungs, gastrointestinal tract, skin, kidney, and retina can lead to multiple degenerative and fatal disorders. It is essential to understand the physiology of the cell barriers to develop more targeted clinical interventions. The discovery, delivery, and development of therapeutic drugs can be facilitated by developing *in vitro* platforms that accurately represent the pathophysiology of the barrier tissues. A framework to verify the sensitivity distribution,

find a geometric correction factor, and test the sensitivity of the model parameters to the output electrical resistance in organ-on-chip devices used for TEER measurement of cell monolayers is presented in this thesis. This work can help to optimize the dimensions and inputs of emerging microfluidic devices for better accuracy of the acquired TEER value, as well as allow comparisons between TEER values collected by different measuring systems.

Bibliography

- [Abbott, 2000] Abbott, N. J. (2000). Inflammatory Mediators and Modulation of Blood-Brain Barrier Permeability. *Cellular and Molecular Neurobiology*, 20(2):131–147. 131.
- [Abbott et al., 2014] Abbott, N. J., Dolman, D. E. M., Yusof, S. R., and Reichel, A. (2014). In Vitro Models of CNS Barriers. In Hammarlund-Udenaes, M., de Lange, E. C., and Thorne, R. G., editors, *Drug Delivery to the Brain: Physiological Concepts, Methodologies and Approaches*, AAPS Advances in the Pharmaceutical Sciences Series, pages 163–197. Springer, New York, NY.
- [Atencia and Beebe, 2005] Atencia, J. and Beebe, D. J. (2005). Controlled microfluidic interfaces. *Nature*, 437(7059):648–655. Number: 7059 Publisher: Nature Publishing Group.
- [Balbuena et al., 2010] Balbuena, P., Li, W., Magnin-Bissel, G., Meldrum, J. B., and Ehrlich, M. (2010). Comparison of Two Blood-Brain Barrier In Vitro Systems: Cytotoxicity and Transfer Assessments of Malathion/Oxon and Lead Acetate. *Toxicological Sciences*, 114(2):260–271.

- [Benson et al., 2013] Benson, K., Cramer, S., and Galla, H.-J. (2013). Impedance-based cell monitoring: barrier properties and beyond. *Fluids and Barriers of the CNS*, 10(1):5.
- [Bol et al., 2013] Bol, L., Galas, J.-C., Hillaireau, H., Le Potier, I., Valérie, N., Haghiri-Gosnet, A.-M., Fattal, E., and Taverna, M. (2013). A microdevice for parallelized pulmonary permeability studies. *Biomedical microdevices*, 16.
- [Brown et al., 2021] Brown, D. G., Wobst, H. J., Kapoor, A., Kenna, L. A., and Southall, N. (2021). Clinical development times for innovative drugs. *Nature Reviews Drug Discovery*.
Bandiera_abtest: a Cg_type: From The Analyst’s Couch Publisher: Nature Publishing Group.
- [Butt et al., 1990] Butt, A. M., Jones, H. C., and Abbott, N. J. (1990). Electrical resistance across the blood-brain barrier in anaesthetized rats: a developmental study. *The Journal of Physiology*, 429(1):47–62.
- [Cho et al., 2002] Cho, C.-W., Liu, Y., Cobb, W. N., Henthorn, T. K., Lillehei, K., Christians, U., and Ng, K.-Y. (2002). Ultrasound-Induced Mild Hyperthermia as a Novel Approach to Increase Drug Uptake in Brain Microvessel Endothelial Cells. *Pharmaceutical Research*, 19(8):1123–1129.
- [Claesson-Welsh et al., 2021] Claesson-Welsh, L., Dejana, E., and McDonald, D. M. (2021). Permeability of the Endothelial Barrier: Identifying and Reconciling Controversies. *Trends in Molecular Medicine*, 27(4):314–331. Publisher: Elsevier.

- [Crone and Christensen, 1981] Crone, C. and Christensen, O. (1981). Electrical resistance of a capillary endothelium. *Journal of General Physiology*, 77(4):349–371.
- [Crone and Olesen, 1982] Crone, C. and Olesen, S. P. (1982). Electrical resistance of brain microvascular endothelium. *Brain Research*, 241(1):49–55.
- [Czupalla et al., 2014] Czupalla, C. J., Liebner, S., and Devraj, K. (2014). In Vitro Models of the Blood–Brain Barrier. In Milner, R., editor, *Cerebral Angiogenesis: Methods and Protocols*, Methods in Molecular Biology, pages 415–437. Springer, New York, NY.
- [Daniels et al., 2013] Daniels, B. P., Cruz-Orengo, L., Pasieka, T. J., Couraud, P.-O., Romero, I. A., Weksler, B., Cooper, J. A., Doering, T. L., and Klein, R. S. (2013). Immortalized human cerebral microvascular endothelial cells maintain the properties of primary cells in an in vitro model of immune migration across the blood brain barrier. *Journal of Neuroscience Methods*, 212(1):173–179.
- [Deli et al., 2005] Deli, M. A., Abrahám, C. S., Kataoka, Y., and Niwa, M. (2005). Permeability studies on in vitro blood-brain barrier models: physiology, pathology, and pharmacology. *Cellular and Molecular Neurobiology*, 25(1):59–127.
- [DiMasi et al., 2016] DiMasi, J. A., Grabowski, H. G., and Hansen, R. W. (2016). Innovation in the pharmaceutical industry: New estimates of R&D costs. *Journal of Health Economics*, 47:20–33.

- [Douville et al., 2010] Douville, N. J., Tung, Y.-C., Li, R., Wang, J. D., El-Sayed, M. E., and Takayama, S. (2010). Fabrication of Two-Layered Channel System with Embedded Electrodes to Measure Resistance Across Epithelial and Endothelial Barriers. *Analytical Chemistry*, 82(6):2505–2511.
- [Duan et al., 2008] Duan, Y., Gotoh, N., Yan, Q., Du, Z., Weinstein, A. M., Wang, T., and Weinbaum, S. (2008). Shear-induced reorganization of renal proximal tubule cell actin cytoskeleton and apical junctional complexes. *Proceedings of the National Academy of Sciences*, 105(32):11418–11423. Publisher: Proceedings of the National Academy of Sciences.
- [Eigenmann et al., 2013] Eigenmann, D. E., Xue, G., Kim, K. S., Moses, A. V., Hamburger, M., and Oufir, M. (2013). Comparative study of four immortalized human brain capillary endothelial cell lines, hCMEC/D3, hBMEC, TY10, and BB19, and optimization of culture conditions, for an in vitro blood–brain barrier model for drug permeability studies. *Fluids and Barriers of the CNS*, 10(1):33.
- [Fang et al., 2004] Fang, X., Song, Y., Zemans, R., Hirsch, J., and Matthay, M. A. (2004). Fluid transport across cultured rat alveolar epithelial cells: a novel in vitro system. *American Journal of Physiology. Lung Cellular and Molecular Physiology*, 287(1):L104–110.

- [Florea et al., 2003] Florea, B. I., Cassara, M. L., Junginger, H. E., and Borchard, G. (2003). Drug transport and metabolism characteristics of the human airway epithelial cell line Calu-3. *Journal of Controlled Release*, 87(1):131–138.
- [Foster et al., 2000] Foster, K. A., Avery, M. L., Yazdanian, M., and Audus, K. L. (2000). Characterization of the Calu-3 cell line as a tool to screen pulmonary drug delivery. *International Journal of Pharmaceutics*, 208(1):1–11.
- [Franke et al., 1999] Franke, H., Galla, H. J., and Beuckmann, C. T. (1999). An improved low-permeability in vitro-model of the blood-brain barrier: transport studies on retinoids, sucrose, haloperidol, caffeine and mannitol. *Brain Research*, 818(1):65–71.
- [Helm et al., 2019] Helm, M. W. v. d., Henry, O. Y. F., Bein, A., Hamkins-Indik, T., Crouce, M. J., Leineweber, W. D., Odijk, M., Meer, A. D. v. d., Eijkel, J. C. T., Ingber, D. E., Berg, A. v. d., and Segerink, L. I. (2019). Non-invasive sensing of transepithelial barrier function and tissue differentiation in organs-on-chips using impedance spectroscopy. *Lab on a Chip*, 19(3):452–463. Publisher: The Royal Society of Chemistry.
- [Hodgkin, 1951] Hodgkin, A. L. (1951). The Ionic Basis of Electrical Activity in Nerve and Muscle. *Biological Reviews*, 26(4):339–409. eprint: <https://onlinelibrary.wiley.com/doi/pdf/10.1111/j.1469-185X.1951.tb01204.x>.

- [Jovov et al., 1991] Jovov, B., Wills, N. K., and Lewis, S. A. (1991). A spectroscopic method for assessing confluence of epithelial cell cultures. *The American Journal of Physiology*, 261(6 Pt 1):C1196–1203.
- [Katz, 1966] Katz, B. (1966). *Nerve, muscle, and synapse*. New York, McGraw-Hill.
- [Khire et al., 2018] Khire, T. S., Nehilla, B. J., Getpreecharsawas, J., Gracheva, M. E., Waugh, R. E., and McGrath, J. L. (2018). Finite Element Modeling to Analyze TEER Values Across Silicon Nanomembranes. *Biomedical microdevices*, 20(1):11.
- [Lang et al., 2015] Lang, Q., Wu, Y., Ren, Y., Tao, Y., Lei, L., and Jiang, H. (2015). AC Electrothermal Circulatory Pumping Chip for Cell Culture. *ACS applied materials & interfaces*, 7.
- [Langen et al., 2019] Langen, U. H., Ayloo, S., and Gu, C. (2019). Development and Cell Biology of the Blood-Brain Barrier. *Annual Review of Cell and Developmental Biology*, 35:591–613.
- [Li et al., 2021] Li, X., Vemireddy, V., Cai, Q., Xiong, H., Kang, P., Li, X., Giannotta, M., Hayenga, H. N., Pan, E., Sirsi, S. R., Mateo, C., Kleinfeld, D., Greene, C., Campbell, M., Dejana, E., Bachoo, R., and Qin, Z. (2021). Reversibly Modulating the Blood–Brain Barrier by Laser Stimulation of Molecular-Targeted Nanoparticles. *Nano Letters*, 21(22):9805–9815. Publisher: American Chemical Society.

- [Linz et al., 2020] Linz, G., Djeljadini, S., Steinbeck, L., Köse, G., Kiessling, F., and Wessling, M. (2020). Cell barrier characterization in transwell inserts by electrical impedance spectroscopy. *Biosensors and Bioelectronics*, 165:112345.
- [Lippmann et al., 2014] Lippmann, E. S., Al-Ahmad, A., Azarin, S. M., Palecek, S. P., and Shusta, E. V. (2014). A retinoic acid-enhanced, multicellular human blood-brain barrier model derived from stem cell sources. *Scientific Reports*, 4(1):4160. Number: 1 Publisher: Nature Publishing Group.
- [Lund and Rosene, 1947] Lund, E. J. and Rosene, H. F. (1947). *Bioelectric fields and growth, with a Bibliography of continuous bioelectric currents and bioelectric fields in animals and plants, by H. F. Rosene*. Univ. of Texas Press, Austin.
- [Lundquist et al., 2002] Lundquist, S., Renftel, M., Brillault, J., Fenart, L., Cecchelli, R., and Dehouck, M.-P. (2002). Prediction of Drug Transport Through the Blood-Brain Barrier in Vivo: A Comparison Between Two in Vitro Cell Models. *Pharmaceutical Research*, 19(7):976–981.
- [Marino et al., 2018] Marino, A., Tricinci, O., Battaglini, M., Filippeschi, C., Mattoli, V., Sinibaldi, E., and Ciofani, G. (2018). A 3D Real-Scale, Biomimetic, and Biohybrid Model of the Blood-Brain Barrier Fabricated through Two-Photon Lithography. *Small*, 14(6):1702959. _eprint: <https://onlinelibrary.wiley.com/doi/pdf/10.1002/sml.201702959>.

- [Mathias et al., 2002] Mathias, N. R., Timoszyk, J., Stetsko, P. I., Megill, J. R., Smith, R. L., and Wall, D. A. (2002). Permeability Characteristics of Calu-3 Human Bronchial Epithelial Cells: In Vitro - In Vivo Correlation to Predict Lung Absorption in Rats. *Journal of Drug Targeting*, 10(1):31–40.
- [Nakagawa et al., 2009] Nakagawa, S., Deli, M. A., Kawaguchi, H., Shimizudani, T., Shimono, T., Kittel, A., Tanaka, K., and Niwa, M. (2009). A new blood-brain barrier model using primary rat brain endothelial cells, pericytes and astrocytes. *Neurochemistry International*, 54(3-4):253–263.
- [Nicolazzo et al., 2006] Nicolazzo, J. A., Charman, S. A., and Charman, W. N. (2006). Methods to assess drug permeability across the blood-brain barrier. *Journal of Pharmacy and Pharmacology*, 58(3):281–293. eprint: <https://onlinelibrary.wiley.com/doi/pdf/10.1211/jpp.58.3.0001>.
- [Nitz et al., 2003] Nitz, T., Eisenblätter, T., Psathaki, K., and Galla, H.-J. (2003). Serum-derived factors weaken the barrier properties of cultured porcine brain capillary endothelial cells in vitro. *Brain Research*, 981(1):30–40.
- [NW et al., 2015] NW, L. S., Washington, S. ., and Inquiries, D. . U.-.-. |. M.-.-. |. F.-.-. |. M. (2015). Chapter 7: Opinion About the Use of Animals in Research.
- [Odijk et al., 2015] Odijk, M., Meer, A. D. v. d., Levner, D., Kim, H. J., Helm, M. W. v. d., Segerink, L. I., Frimat, J.-P., Hamilton, G. A., Ingber, D. E., and Berg, A. v. d.

- (2015). Measuring direct current trans-epithelial electrical resistance in organ-on-a-chip microsystems. *Lab on a Chip*, 15(3):745–752. Publisher: The Royal Society of Chemistry.
- [Pardridge, 2004] Pardridge, W. M. (2004). Log(BB), PS products and in silico models of drug brain penetration. *Drug Discovery Today*, 9(9):392–393.
- [Perel et al., 2007] Perel, P., Roberts, I., Sena, E., Wheble, P., Briscoe, C., Sandercock, P., Macleod, M., Mignini, L. E., Jayaram, P., and Khan, K. S. (2007). Comparison of treatment effects between animal experiments and clinical trials: systematic review. *BMJ*, 334(7586):197. Publisher: British Medical Journal Publishing Group Section: Research.
- [Pouliopoulos et al., 2020] Pouliopoulos, A. N., Wu, S.-Y., Burgess, M. T., Karakatsani, M. E., Kamimura, H. A. S., and Konofagou, E. E. (2020). A Clinical System for Non-invasive Blood-Brain Barrier Opening Using a Neuronavigation-Guided Single-Element Focused Ultrasound Transducer. *Ultrasound in Medicine & Biology*, 46(1):73–89.
- [Prabhakarandian et al., 2013] Prabhakarandian, B., Shen, M.-C., Nichols, J. B., Mills, I. R., Sidoryk-Wegrzynowicz, M., Aschner, M., and Pant, K. (2013). SyM-BBB: A Microfluidic Blood Brain Barrier Model. *Lab on a chip*, 13(6):1093–1101.
- [Shen et al., 1994] Shen, B. Q., Finkbeiner, W. E., Wine, J. J., Mrsny, R. J., and Widdicombe, J. H. (1994). Calu-3: a human airway epithelial cell line that shows cAMP-dependent Cl⁻ secretion. *The American Journal of Physiology*, 266(5 Pt 1):L493–501.

- [Shin et al., 2020] Shin, D. W., Fan, J., Luu, E., Khalid, W., Xia, Y., Khadka, N., Bikson, M., and Fu, B. M. (2020). In Vivo Modulation of the Blood–Brain Barrier Permeability by Transcranial Direct Current Stimulation (tDCS). *Annals of Biomedical Engineering*, 48(4):1256–1270.
- [Smith and Rapoport, 2006] Smith, Q. R. and Rapoport, S. I. (2006). Cerebrovascular Permeability Coefficients to Sodium, Potassium, and Chloride. *Journal of Neurochemistry*, 46(6):1732–1742.
- [Srinivasan et al., 2015] Srinivasan, B., Kolli, A. R., Esch, M. B., Abaci, H. E., Shuler, M. L., and Hickman, J. J. (2015). TEER measurement techniques for in vitro barrier model systems. *Journal of laboratory automation*, 20(2):107–126.
- [status report, 2021] status report, W. G. (2021). Dementia. Technical report.
- [Ussing, 1980] Ussing, H. H. (1980). Life with Tracers. *Annual Review of Physiology*, 42(1):1–17.
- [Ussing and Zerahn, 1951] Ussing, H. H. and Zerahn, K. (1951). Active transport of sodium as the source of electric current in the short-circuited isolated frog skin. *Acta Physiologica Scandinavica*, 23(2-3):110–127.
- [van der Helm et al., 2016] van der Helm, M. W., Odijk, M., Frimat, J.-P., van der Meer, A. D., Eijkel, J. C. T., van den Berg, A., and Segerink, L. I. (2016). Direct quantification

of transendothelial electrical resistance in organs-on-chips. *Biosensors & Bioelectronics*, 85:924–929.

[Walker et al., 2004] Walker, G. M., Zeringue, H. C., and Beebe, D. J. (2004). Microenvironment design considerations for cellular scale studies. *Lab on a Chip*, 4(2):91.

[Wang et al., 2017] Wang, Y. I., Abaci, H. E., and Shuler, M. L. (2017). Microfluidic blood-brain barrier model provides in vivo-like barrier properties for drug permeability screening. *Biotechnology and Bioengineering*, 114(1):184–194.

[Weiss et al., 2009] Weiss, N., Miller, F., Cazaubon, S., and Couraud, P.-O. (2009). The blood-brain barrier in brain homeostasis and neurological diseases. *Biochimica et Biophysica Acta (BBA) - Biomembranes*, 1788(4):842–857.

[Wilhelm et al., 2011] Wilhelm, I., Fazakas, C., and Krizbai, I. A. (2011). In vitro models of the blood-brain barrier. *Acta Neurobiologiae Experimentalis*, 71(1):113–128.

[Yeste et al., 2016] Yeste, J., Illa, X., Gutiérrez, C., Solé, M., Guimerà, A., and Villa, R. (2016). Geometric correction factor for transepithelial electrical resistance measurements in transwell and microfluidic cell cultures. *Journal of Physics D: Applied Physics*, 49(37):375401. Publisher: IOP Publishing.

[Zonta et al., 2003] Zonta, M., Angulo, M. C., Gobbo, S., Rosengarten, B., Hossmann, K.-A., Pozzan, T., and Carmignoto, G. (2003). Neuron-to-astrocyte signaling is central to the dynamic control of brain microcirculation. *Nature Neuroscience*, 6(1):43–50.